Introduction to Gamma-ray Burst Astrophysics

Jakub Řípa
Astronomical Institute of Charles University
MTA-Eötvös Loránd University, Budapest

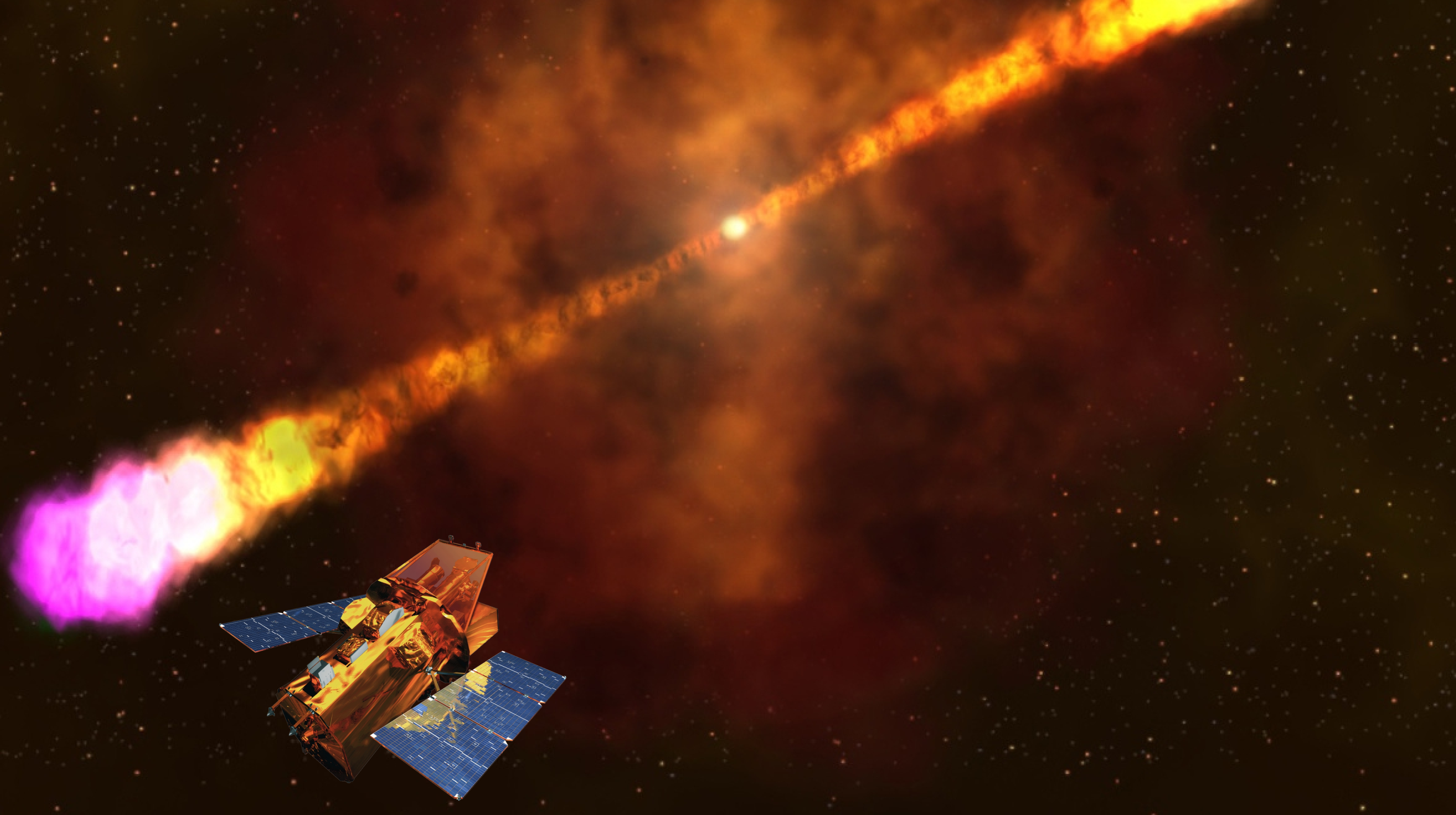

Correlations Between Spectral and/or Temporal Properties and Energetics of GRBs

Relation: L_{iso} vs spectral lag τ_{lag}

- Anti-correlation between isotropic equivalent luminosity L_{iso} and spectral lag τ_{lag} (Norris et al. 2000; Schaefer et al. 2001).

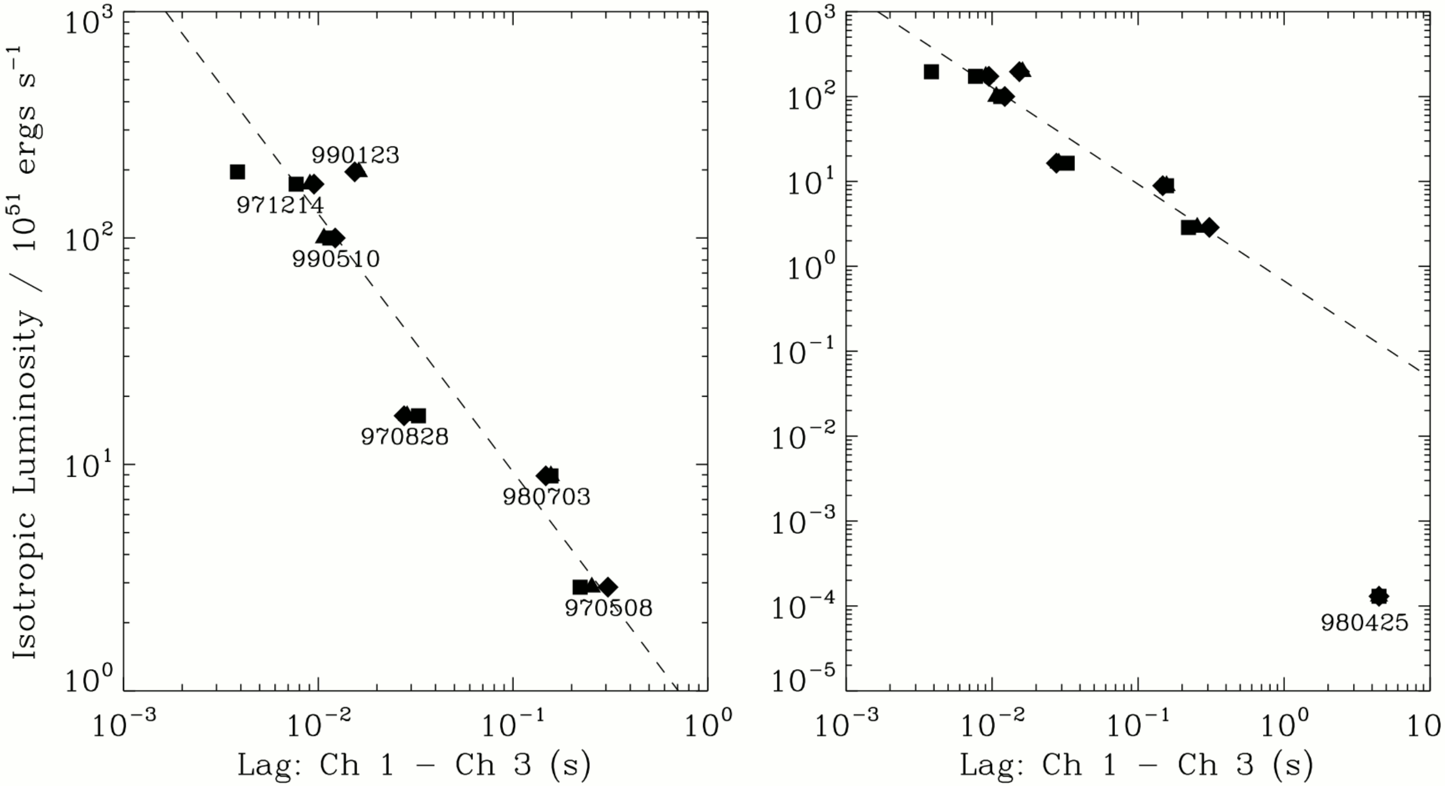

FIG. 6.—Left-hand panel is the same as lower right-hand panel of Fig. 2, but with log-log coordinates for CCF31 lag vs. peak luminosity, for the subset of six bursts with known redshifts. The dashed line is a power-law fit to the lags for intervals including count rates greater than 0.1 × peak intensity (*squares*), yielding $L_{53} \approx 1.3 \times (\tau/0.01\ \mathrm{s})^{-1.14}$. In the right-hand panel, the luminosity range is expanded to include GRB 980425 (assuming a connection with SN 1998bw), which falls below the extrapolated power law by a factor of ~400–700, depending on the precise power-law slope adopted.

Norris et al. 2000

- Correlation between L_{iso} and light-curve variability V (Fenimore and Ramirez-Ruiz 2000; Reichart et al. 2001; Li and Paczynski 2006).
- V does correlate with *L*, but very large scatter.

$$L_{iso} \sim V^{3.3}$$

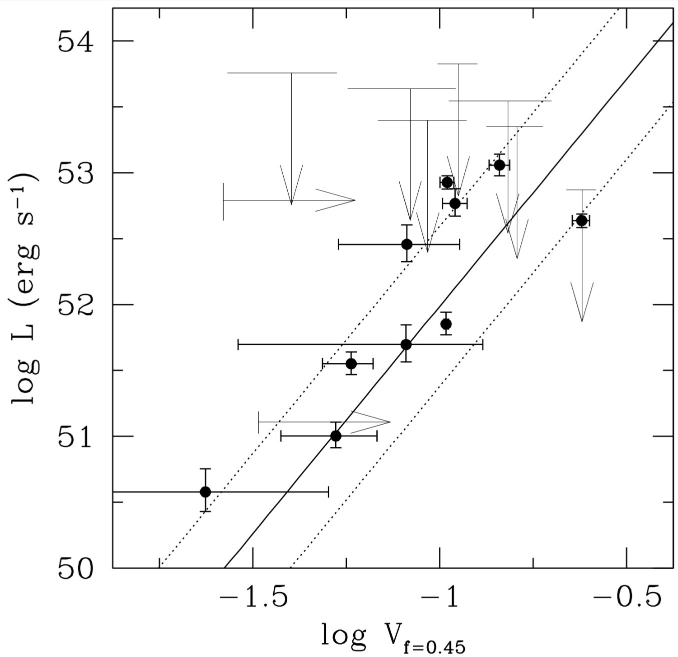

FIG. 9.—Variabilities $V_{f=0.45}$ and isotropic equivalent peak luminosities L of the bursts in our sample, excluding GRB 980425. Solid and dotted lines mark the center and 1 σ widths of the best-fit model distribution of these bursts in the log L–log $V_{f=0.45}$ plane.

Reichart et al. 2001

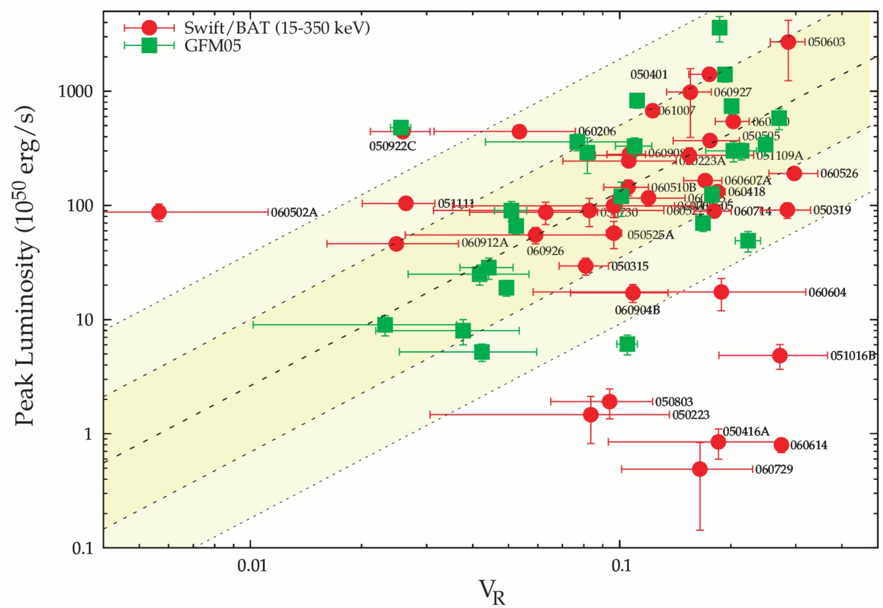

Enriched sample (BSAX+Swift-BAT GRBs (Rizzuto et al. 2007).

Amati Relation: E_p vs E_{iso}

- From redshift, fluence and spectrum, it is possible to estimate the cosmological rest frame peak energy E_p and the radiated energy assuming isotropic emission E_{iso}.
- Correlation between source rest frame peak energy E_p of the prompt gamma spectrum and isotropic equivalent energy E_{iso}.
- First reported by Amati et al. 2002 using the sample of the BeppoSAX satellite with GRBs with measured redshift. Later confirmed on larger samples Amati et al. (2006, 2009, 2015).

$$E_p \sim E_{iso}^{0.5}$$

- $E_{\rm p} = E_{\rm p,obs(1+z)}$ Intrinsic peak energy of time-integrated energy spectrum.
- $E_{\rm iso} = \frac{4\pi d_1^2}{1+z} T_{90} \int_{\frac{1\rm keV}{1+z}}^{\frac{10^4\rm keV}{1+z}} EN(E)dE$ Isotropic energy release over T_{90} in 1 keV – 10 MeV.

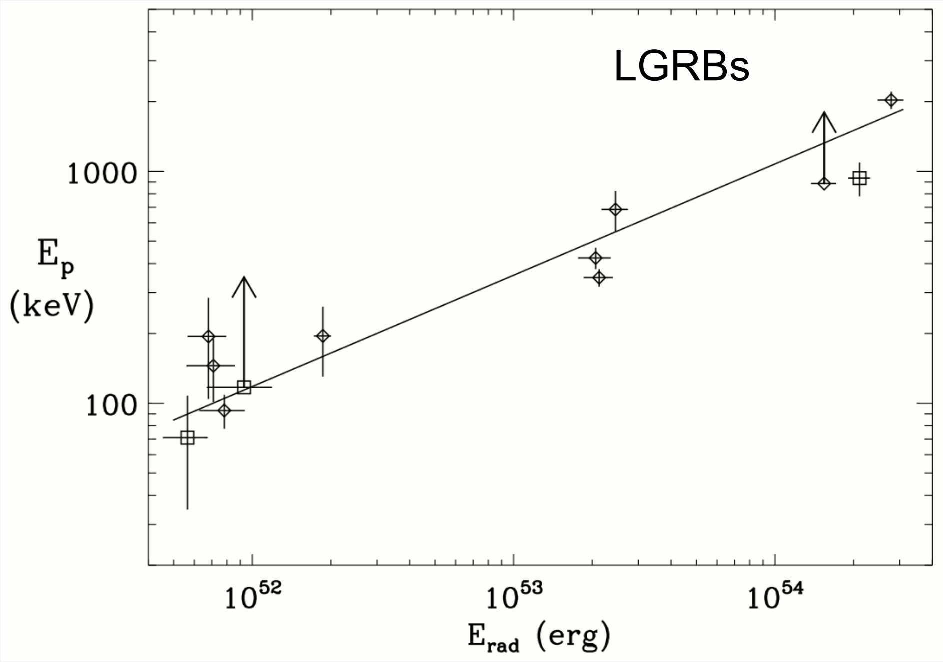

Amati et al. 2002

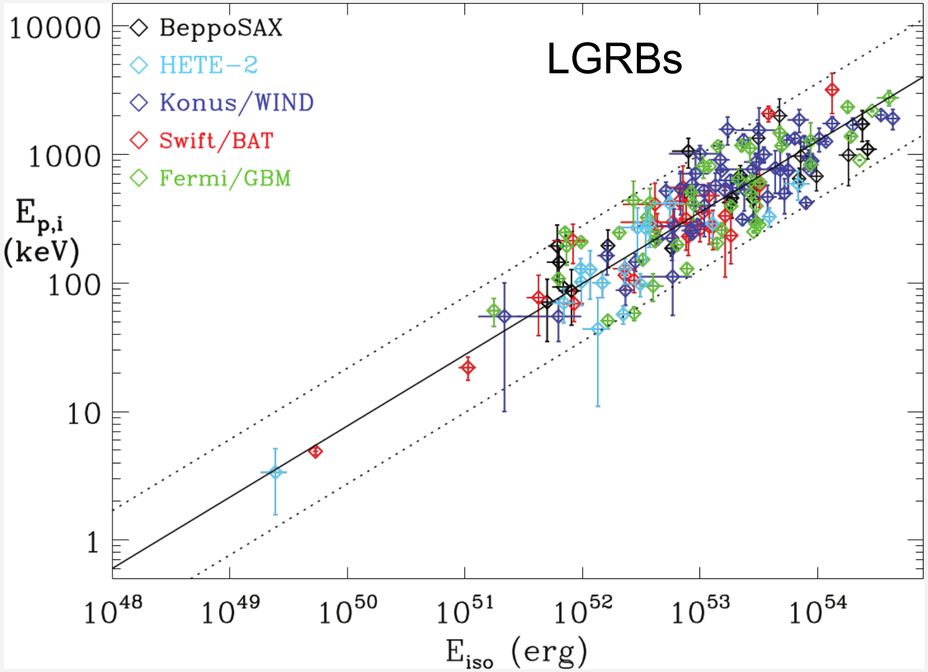

Amati & Valle 2015

Amati Relation: E_p vs E_{iso}

- The correlation holds also for short duration GRBs.

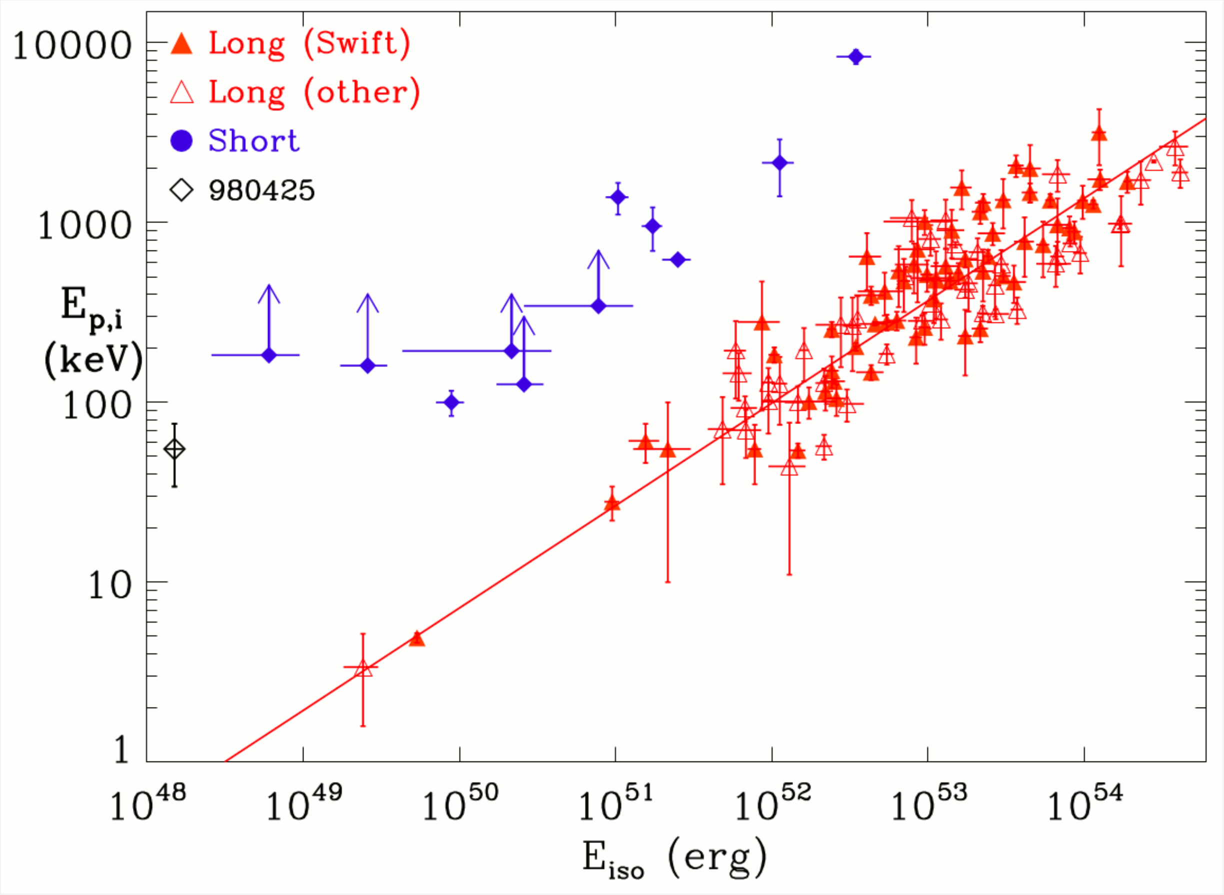

GRBs in the $E_{p,i}$ - E_{iso} plane as of end of 2009. The continuous line is the best fit power-law of the 108 long GRBs (Amati et al. 2010).

Yonetoku Relation: E_p vs L_p

- Correlation between source rest frame peak energy E_p of the prompt gamma spectrum and isotropic equivalent peak luminosity L_p (Yonetoku et al. 2004, 2010).

$$E_p \sim L_p^{1.6}$$

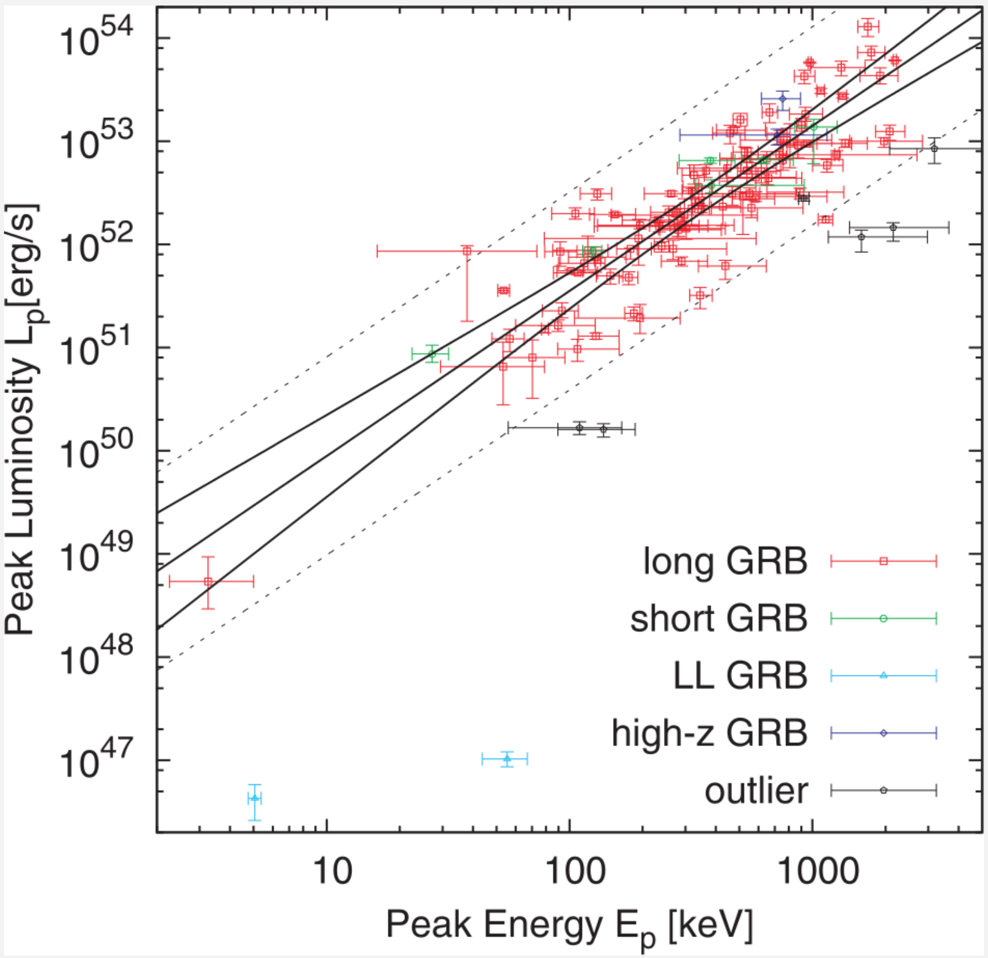

Yonetoku et al. 2010

Ghirlanda Relation: E_p vs E_γ

- Correlation between source rest frame peak energy E_p of the of the prompt gamma spectrum and collimated energy released E_γ (Ghirlanda et al. 2004, 2006; Nava et al. 2006).
- Similar to Amati relation but less scatterd.

$$E_p \sim E_\gamma^{0.7}$$

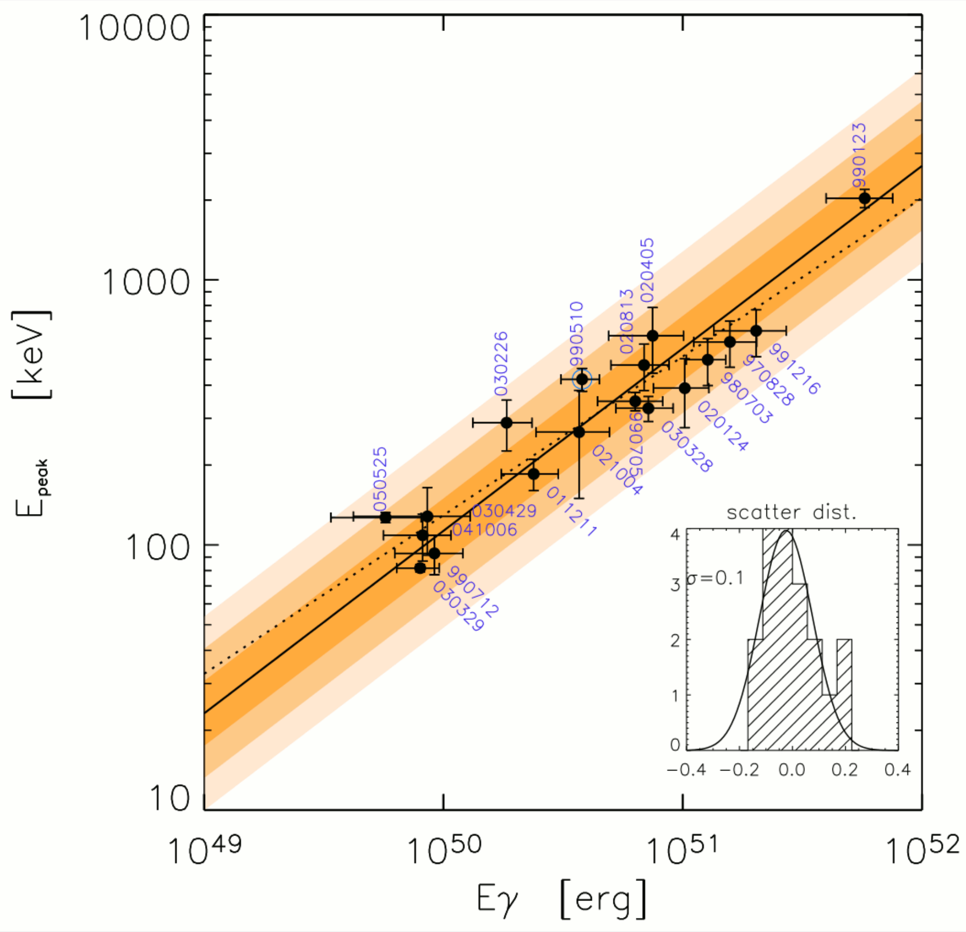

Nava et al. 2006

Other Correlations

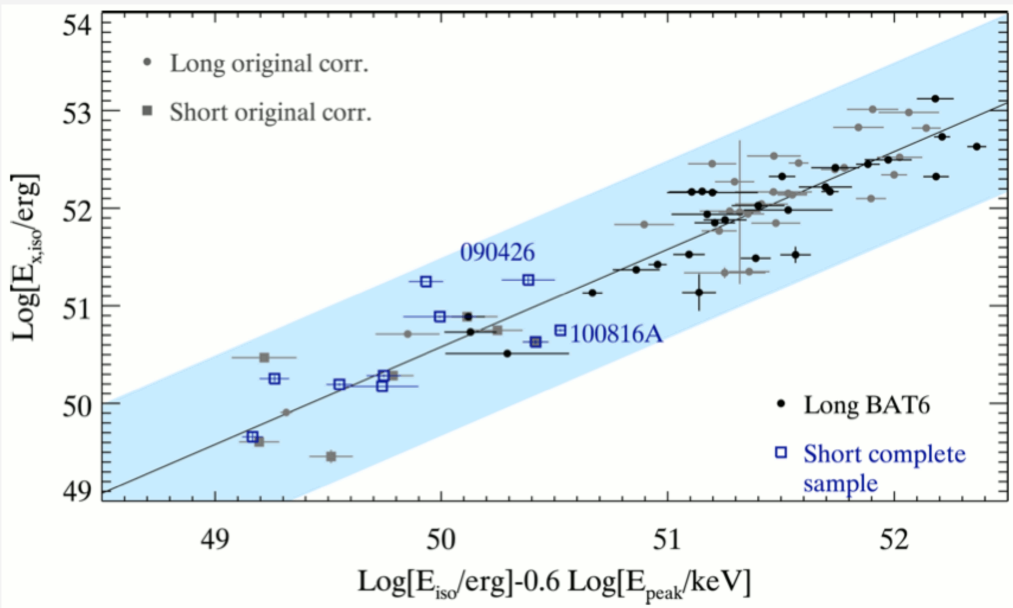

Bernardini et al. 2012; Margutti et al. 2012

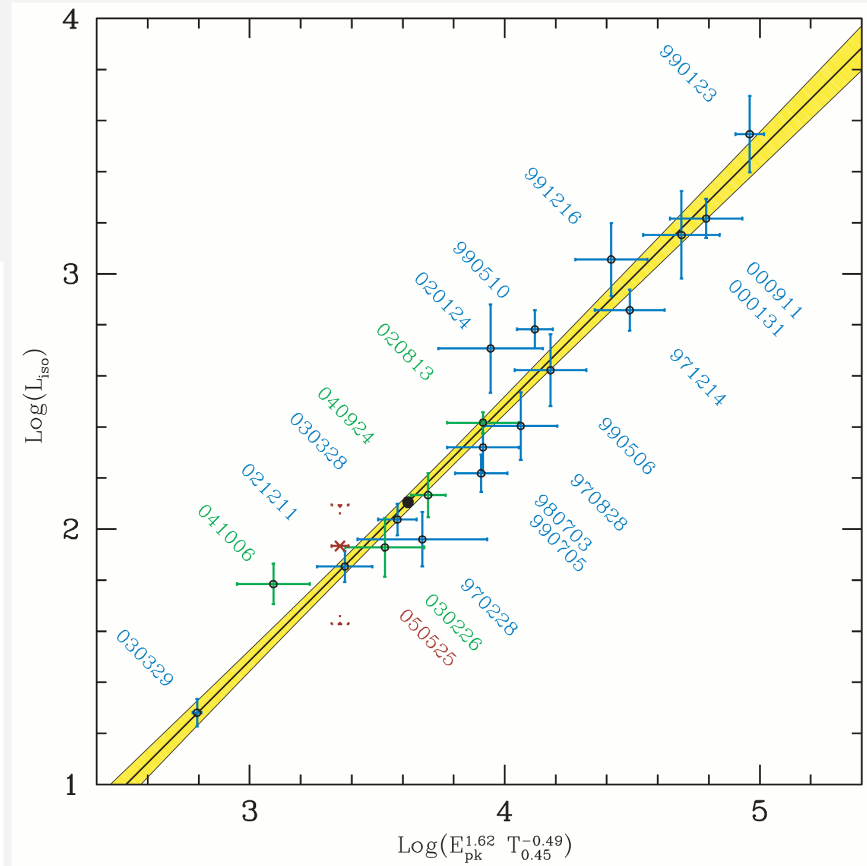

Correlation between E_p-L_{iso}-$T_{0.45}$ where $T_{0.45}$ is the time spanned by the brightest 45% of the total counts above the background (Firmani et al. 2006).

- There are also other correlation, see a review paper Dainotti et al. 2018.

Pseudo-redshifts

Pseudo-redshifts

- If we assume that a given correlation between spectral or temporal properties of GRB light curves and intrinsic luminosity or total emitted energy, e.g. Amati relation, holds then from measured, e.g. $E_{p,obs}$, fluence S, a pseudo-redshift can be calculated.
- See e.g. Atteia 2003; Kocevski and Liang 2003; Ghirlanda et al. 2005; Guidorzi 2005; Guidorzi et al. 2006; Tsutsui et al. 2008, 2013; Zhang and Wang 2018; Zitouny et al. 2018.

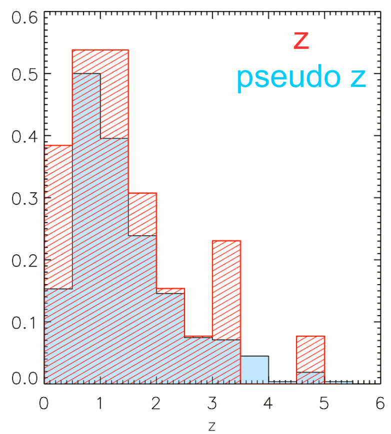

Figure 1. Redshift distribution of the sample of bursts with pseudo-redshift (filled histogram, 442 objects), compared to the redshift distribution of GRBs with measured spectroscopic redshift (red-hatched histogram, 27 objects). Distributions are normalized.

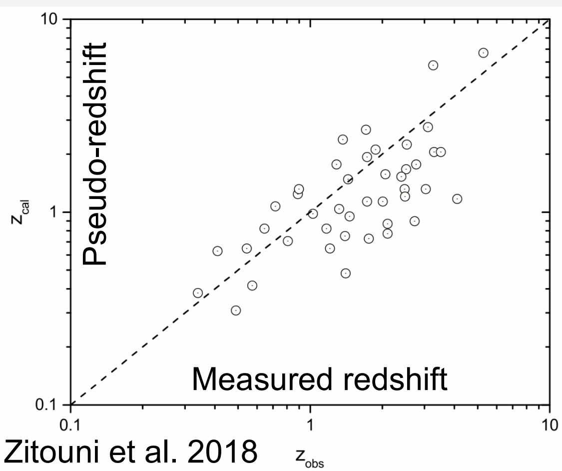

Zitouni et al. 2018

Fig. 8 z_{cal} vs. z_{obs} for the 43 GRBs with $\frac{\Delta z}{z} < 0.8$

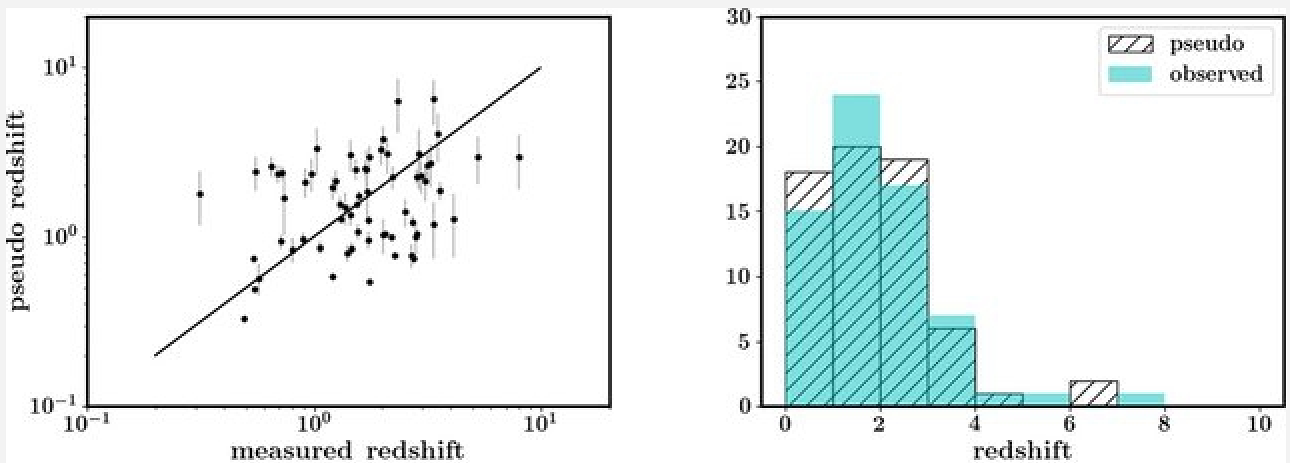

Sample of long gamma-ray bursts (GRBs) common to both Swift and Fermi to re-derive the parameters of the Yonetoku correlation (Paul 2017).

GRBs as Cosmological Tools

GRBs as Cosmological Tools

- These correlations can be used as cosmological tools to construct Hubble diagram (distance modulus vs. redshift) and to constrain cosmological parameters.
- For measured z, S, $E_{\rm p,obs}$ of many GRBs:

$$d_{\rm l} = d_{\rm l}(E_{\rm p,obs}, S, z)$$

$$\mu(z) = 5\log\left(\frac{d_{\rm l}}{\rm Mpc}\right) + 25$$

$$\chi^2(\Omega_M, \Omega_\Lambda) = \sum_{i=1}^{N} \frac{\left[\mu(z_i) - \mu^{\rm pred}(z_i, H_0, \Omega_M, \Omega_\Lambda)\right]^2}{\sigma^2_{\mu(z_i)}}$$

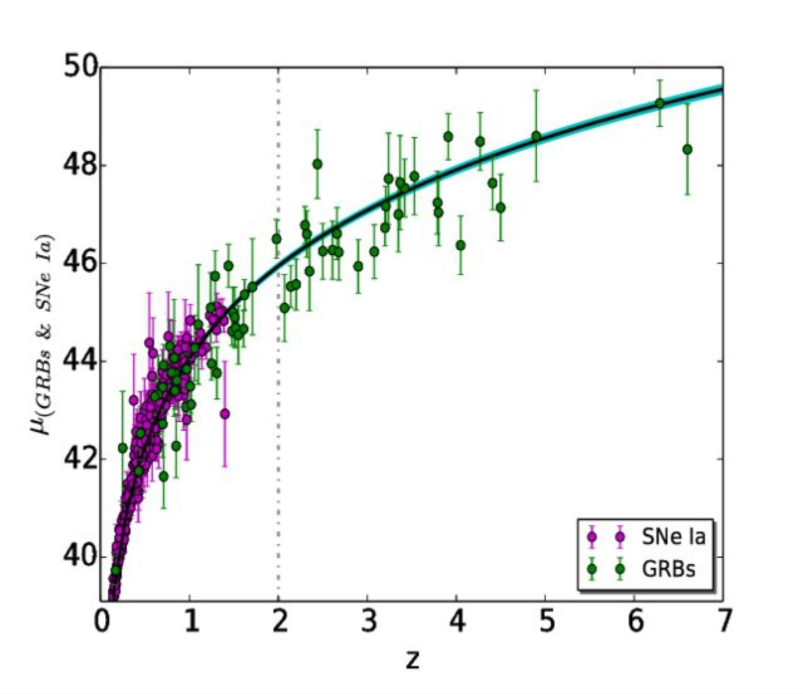

The Hubble diagram of 67 GRBs (green) and 557 SNe Ia (magenta) by Dirirsa and Razzaque 2015.

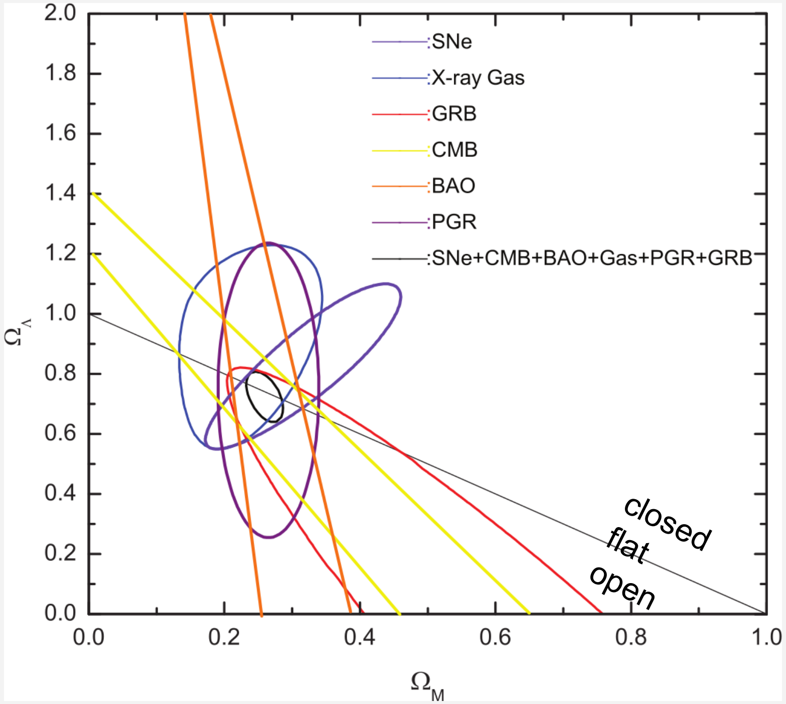

Constraint on ΛCDM model. Joint 1σ confidence intervals given by constraints from the datasets of galaxy clusters, GRBs, CMB shift parameter, SNe Ia, BAO, and 2dF Galaxy Redshift Survey (Wang et al. 2007, 2015).

GRBs as Probes of High-Redshift Universe

GRBs Probing High-z Universe

- GRBs are seen out to high redshift (>5) allowing us to prob high-z universe.

High Redshift GRBs

z	Look-Back Time (Gyr)	GRB	Optical Brightness
9.4	13.1	090429B	K = 19
8.2	13.0	090423	K = 20
~8	13.0	120923A	
7.5	13.0	100905A	H ~ 19
6.7	12.8	080813	K = 19
6.3	12.8	050904	J = 18
6.2	12.8	120521C	
5.6	12.6	060927	I = 16
5.3	12.6	050814	K = 18
5.11	12.5	060522	R = 21

Gehrels 2014

History of the Universe

Redshift	Time
1000 -	
100 -	17 Myr
10 -	480 Myr
9.4 GRB 090429B	
5 -	1.2 Gyr
0.5 -	8.7 Gyr
0 -	13.7 Gyr

Big Bang - Hot ionized gas

The Universe becomes neutral and opaque

Stars and galaxies form
Reionization starts

Cosmic Renaissance
Dark Ages end

Reionization complete $z \approx 6$

Galaxies evolve

Solar System forms

Djorgovski et al.

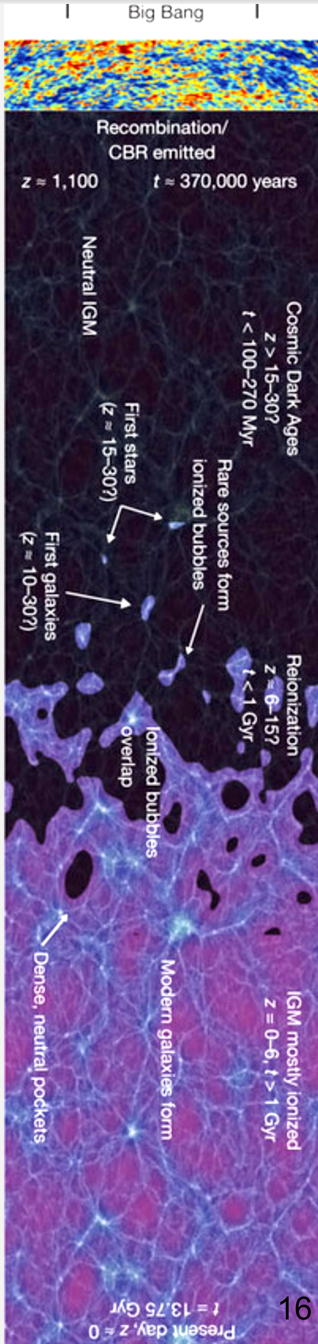

Evolution of Metallicity with Redshift

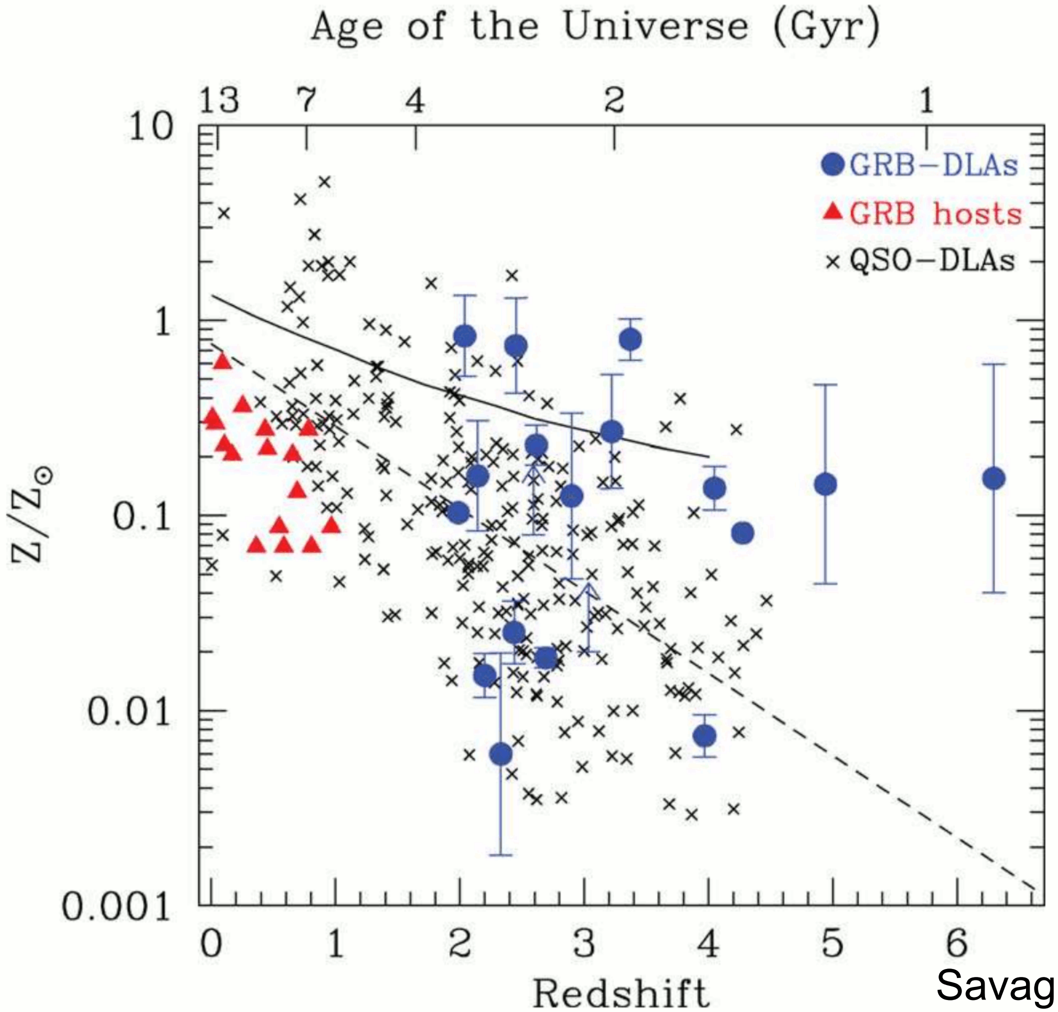

Savaglio 2010

Figure 2. Redshift evolution of the metallicity relative to solar values, for 17 GRB-DLAs at $z > 2$, 16 GRB hosts at $z < 1$ and ~ 250 QSO-DLAs in the interval $0 < z < 4.4$. Error bars are not available for all GRB-DLAs. Errors for GRB hosts are not estimated. Errors for QSO-DLAs are generally smaller than 0.2 dex. The dashed line is the best-fit linear correlation for QSO-DLAs. The solid line is the mean metallicity predicted by semi-analytic models for galaxy formation (Somerville *et al.* 2001). The GRB-DLAs metallicity in $2 < z < 4.5$ is on average 2.5 times higher than the average value in QSO-DLAs in the same redshift interval.

Star Formation Rate Density of the Universe

- GRBs allow to trace the total mass of stars formed per year in a given volume (star formation rate density) at high redshift.
- Rapidly increases at z<1, remains almost constant in the redshift range 1<z<4, and then shows a steep decline with slope at z ~4. The sharp drop at z ~4 may be due to significant dust extinction (Wei et al. 2014).

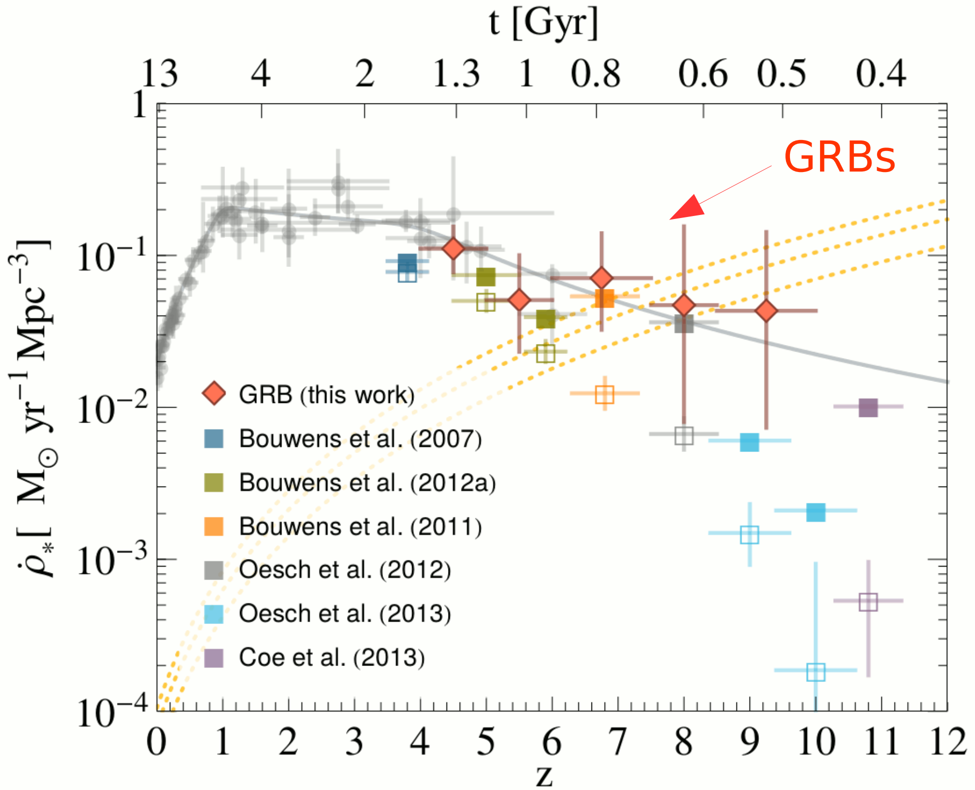

FIG. 1.— The cosmic star formation history. Low-z data (*circles*) are from the compilation of Hopkins & Beacom (2006). The *diamonds* are our values obtained using *Swift* gamma-ray bursts. The *open squares* show the result of integrating the LBG UV luminosity functions down to the lowest measured value, $M_{\rm vis}$, while the *solid squares* use $M_{\rm cut} = -10$ (see Table 1). All assume a Salpeter IMF. For comparison, we show the critical $\dot{\rho}_*$ from Madau et al. (1999) for $\mathcal{C}/f_{\rm esc} = 40,\ 30,\ 20$ (*dotted lines*, top to bottom).

Kistler et al. 2013

- Gunn-Peterson trough is a feature of the spectra of very distant objects (quasars, GRBs) due to the presence of neutral hydrogen (HI) in the Intergalactic Medium (Gunn & Peterson 1965).
- It is suppression of electromagnetic waves from the source at wavelengths less than the Lyman-alpha line at the redshift of the emitted light.
- Observational test for a smoothly distributed neutral Intergalactic Medium.

Searching for the red damping wing in GRB afterglow spectra

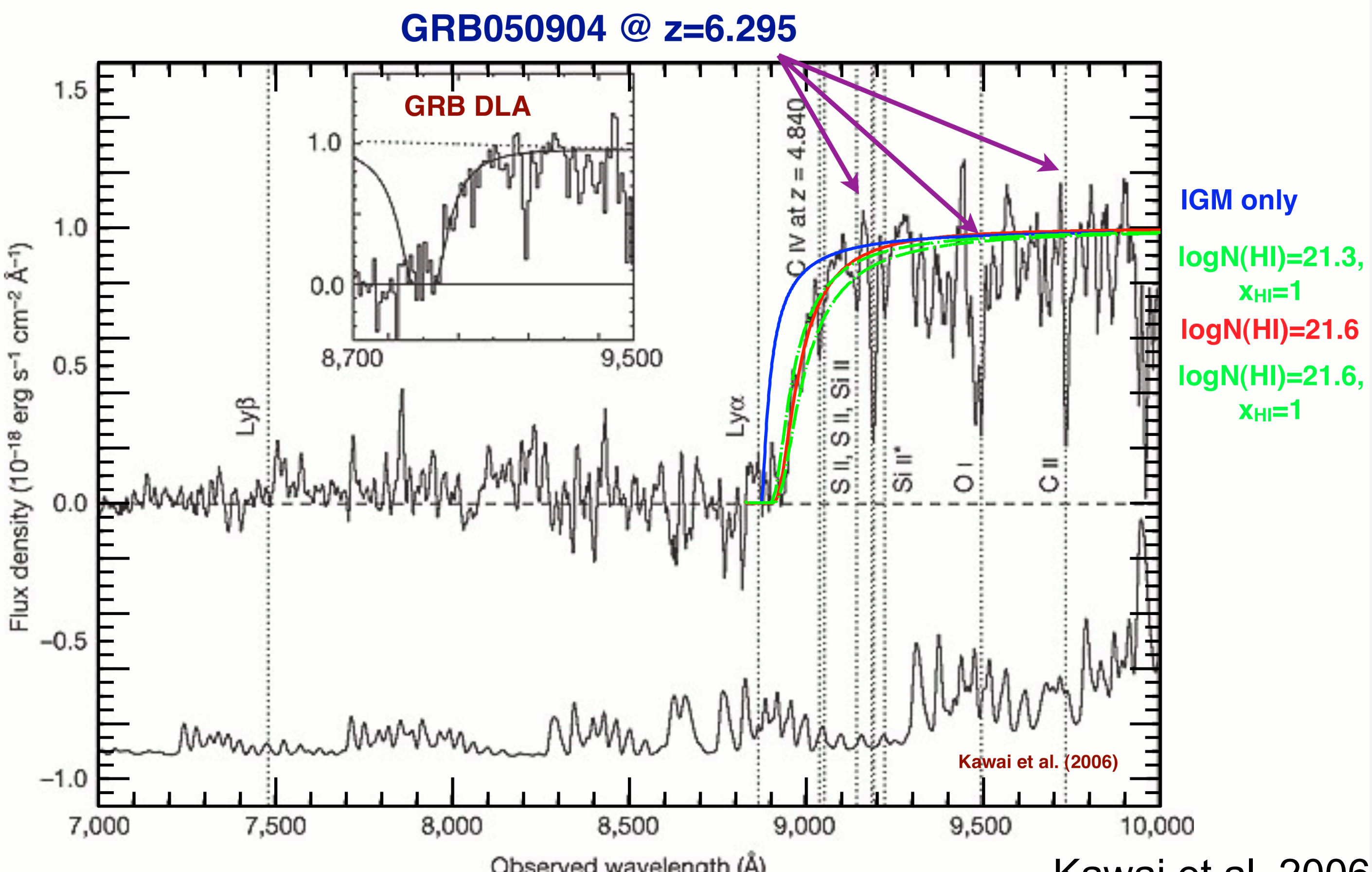

Kawai et al. 2006

GRBs from Population III Stars?

GRBs from Population III Stars?

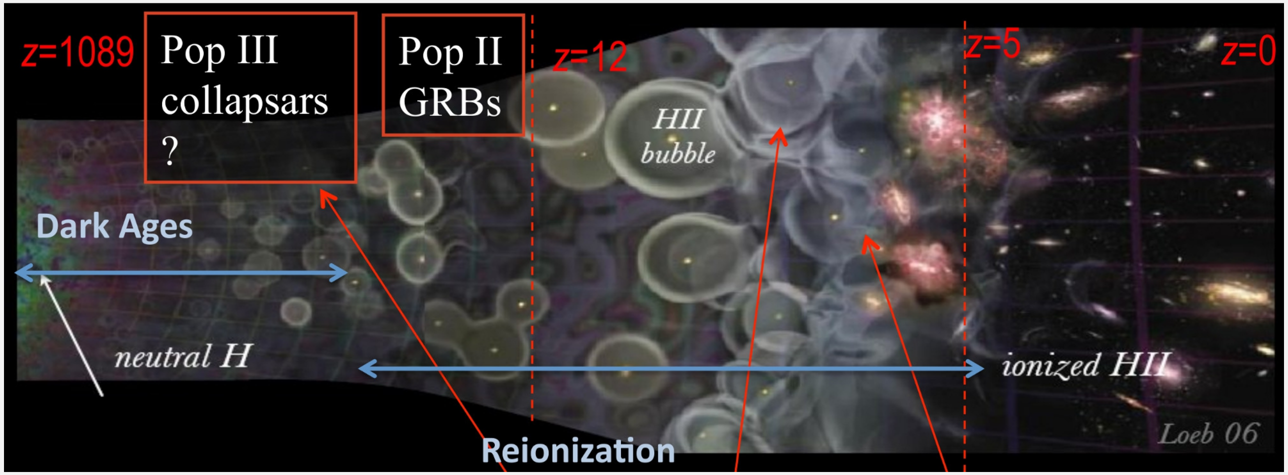

- Possible masses of Pop III stars around ≥ 100 M_{solar}
- Composed entirely of primordial gas, metal-free, mainly hydrogen and helium.
- Expectations of such GRBs are duration T_{90}~1000-10 000 s, $E_{iso}=10^{55}$ erg, $L=10^{52}$ erg/s
- At redshift ~20
- Abel et al. 2002; Bromm et al. 2002; Mészáros and Rees 2010
- No observation so far.

GRBs from Population III Stars?

- Another work claims that hydrodynamic simulations suggest that Pop III stars were formed as binaries or as small multiple systems with stellar masses 10 to 40 M_{solar}.

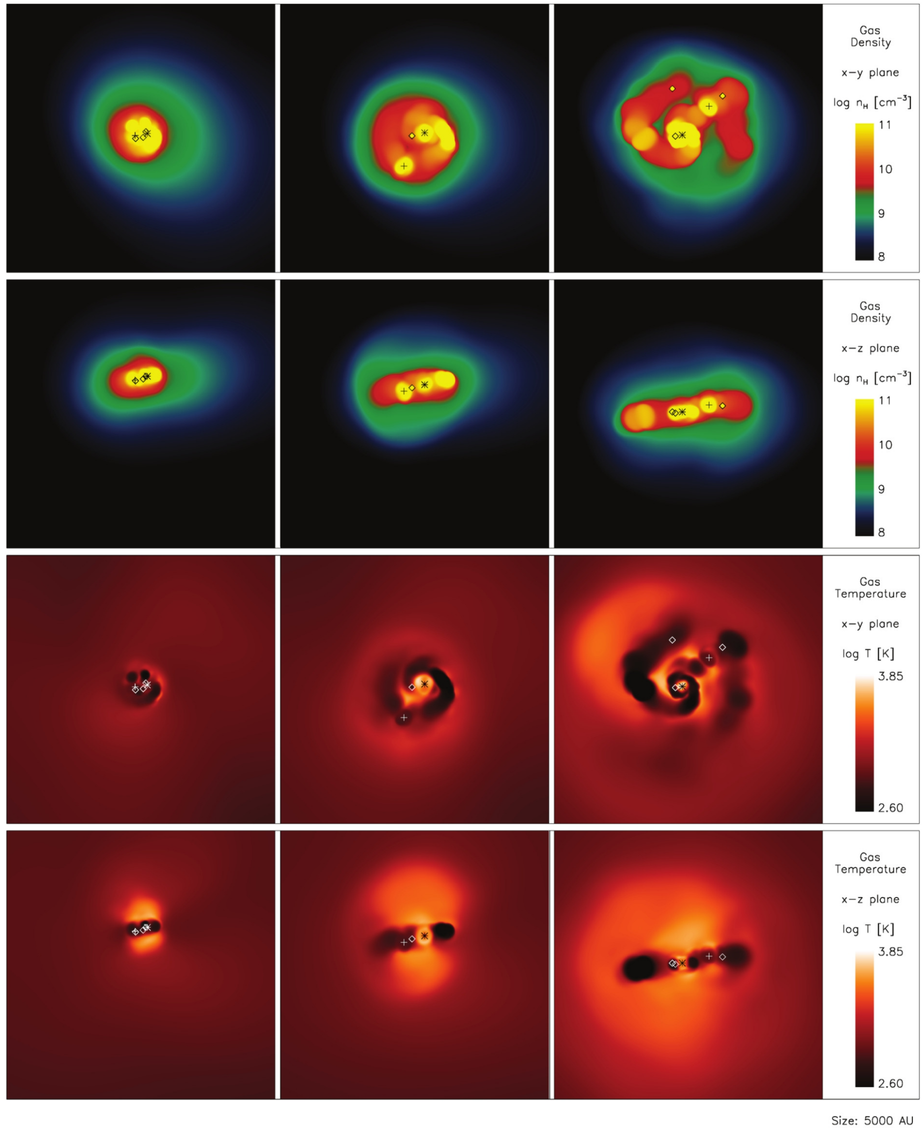

Figure 5. Density and temperature projections of the central 5000 au. Each row shows the projections at 1000 yr (left), 2000 yr (centre) and 5000 yr (right) after the initial sink formation. Asterisks denote the location of the most massive sink. Crosses show the location of the second most massive sink. Diamonds are the locations of the other sinks. Top row: density structure of the central region in the *x-y* plane. Second row: density structure of the central region in the *x-z* plane. Third row: temperature structure of the central region in the *x-y* plane. Bottom row: temperature structure of the central region in the *x-z* plane.

Stacy et al. 2010

GRBs from Population III Stars?

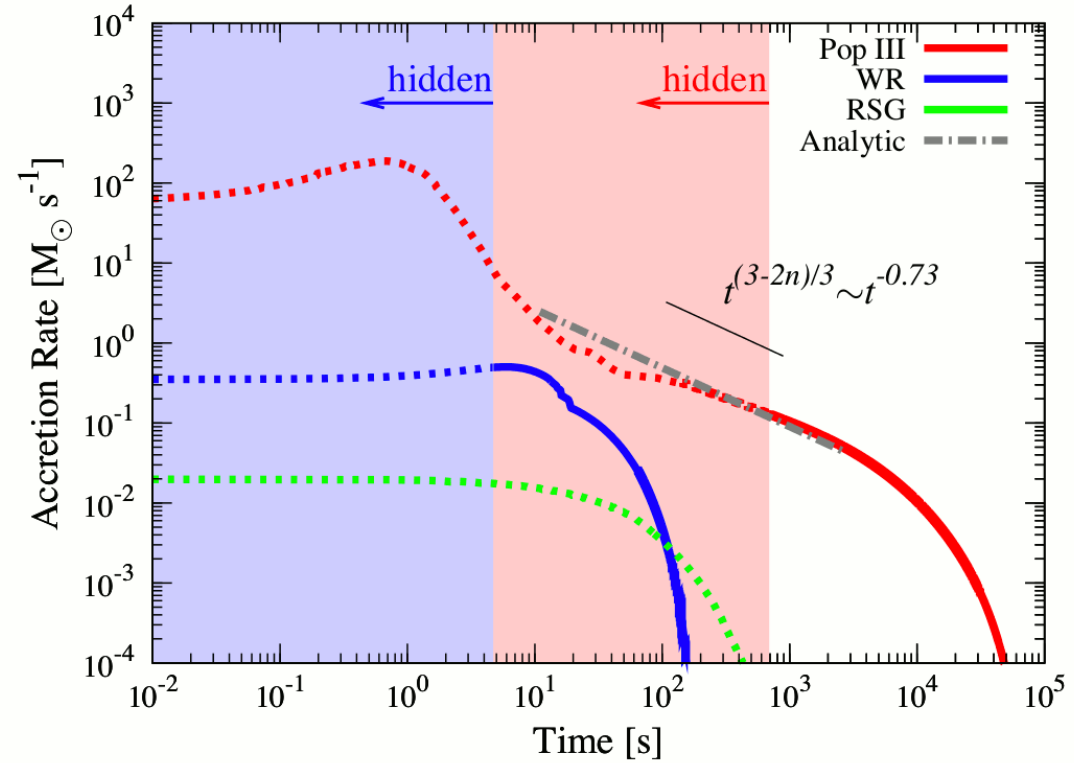

Figure 2. Accretion rates as a function of time. Red, blue, and green lines show Pop III, W-R, and RSG, respectively. Dotted regions represent the jet that propagates inside the star, while the solid regions correspond to the time after the jet breakout for the magnetic jet model. Solid lines give information of observables (e.g., duration and energetics of the GRB). On the other hand, dotted regions show the hidden energy inside the star that goes into the nonrelativistic cocoon component. The gray dot-dashed line represents the analytic model in Equation (13). The black line shows $t^{(3-2n)/3} \sim t^{-0.73}$ as a reference, where $n \sim 2.6$ is a parameter for the density profile (an effective polytropic index of the envelope; see Section 6).

Suwa & Ioka 2011

- Shock breakout is possible even in a massive, metal-free Pop III stars with a large H envelope thanks to the longlived powerful accretion of the envelope.

GRBs from Population III Stars?

- Expected star-formation rate and GRB rate for Pop I, II and III stars.

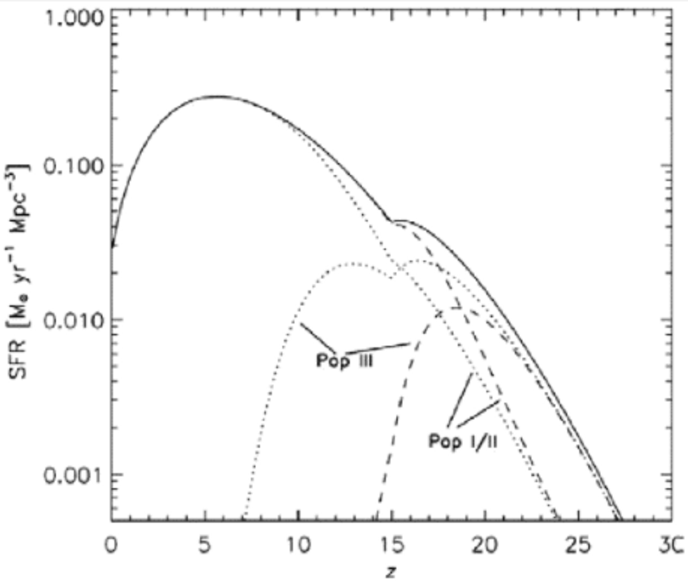

Fig. 14.8. Cosmic star-formation rate (SFR) in units of $M_\odot\ yr^{-1}$ (comoving Mpc)$^{-3}$, as a function of redshift (from Bromm & Loeb 2006). We assume that cooling in primordial gas is due to atomic hydrogen only, a star-formation efficiency of $\eta_* = 10\%$, and reionization beginning at $z_{\rm reion} \approx 17$. Solid line: Total comoving SFR. Dotted lines: Contribution to the total SFR from Pop I/II and Pop III for the case of weak chemical feedback. Dashed lines: Contribution to the total SFR from Pop I/II and Pop III for the case of strong chemical feedback. Pop III star formation is restricted to high redshifts, but extends over a significant range, $\Delta z \sim 10$–15. (Reproduced with permission from the AAS.)

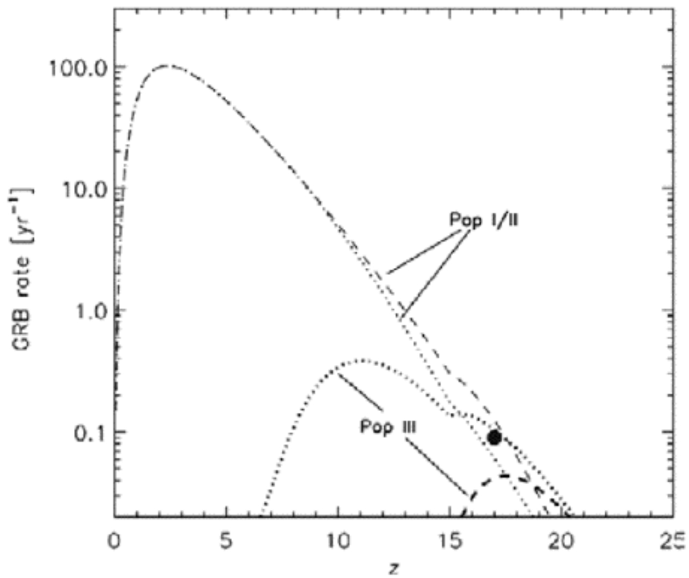

Fig. 14.9. Predicted GRB rate to be observed by *Swift* (from Bromm & Loeb 2006). Shown is the observed number of bursts per year, $dN^{\rm obs}_{\rm GRB}/d\ln(1+z)$, as a function of redshift. All rates are calculated with a constant GRB efficiency, $\eta_{\rm GRB} \simeq 2 \times 10^{-9}$ bursts $M_\odot^{-1}$, using the cosmic SFRs from the previous figure. Dotted lines: Contribution to the observed GRB rate from Pop I/II and Pop III for the case of weak chemical feedback. Dashed lines: Contribution to the GRB rate from Pop I/II and Pop III for the case of strong chemical feedback. Filled circle: GRB rate from Pop III stars if these were responsible for reionizing the Universe at $z \sim 17$. (Reproduced by permission of the AAS.)

Kouveliotou et al 2012;
Bromm and Loeb 2006

Multi-Messenger Observations - UHECR, Neutrinos, GW

Possible Neutrino Production Sites

- GRBs were proposed to be sites for accelerating ultra-high energy cosmic rays and sources of very high energy neutrinos up to 10^{17}~10^{19} eV (Waxman and Bahcall 1997, 2000; P. Mészáros Waxman 2001; Waxman 2003; P. Mészáros 2015).

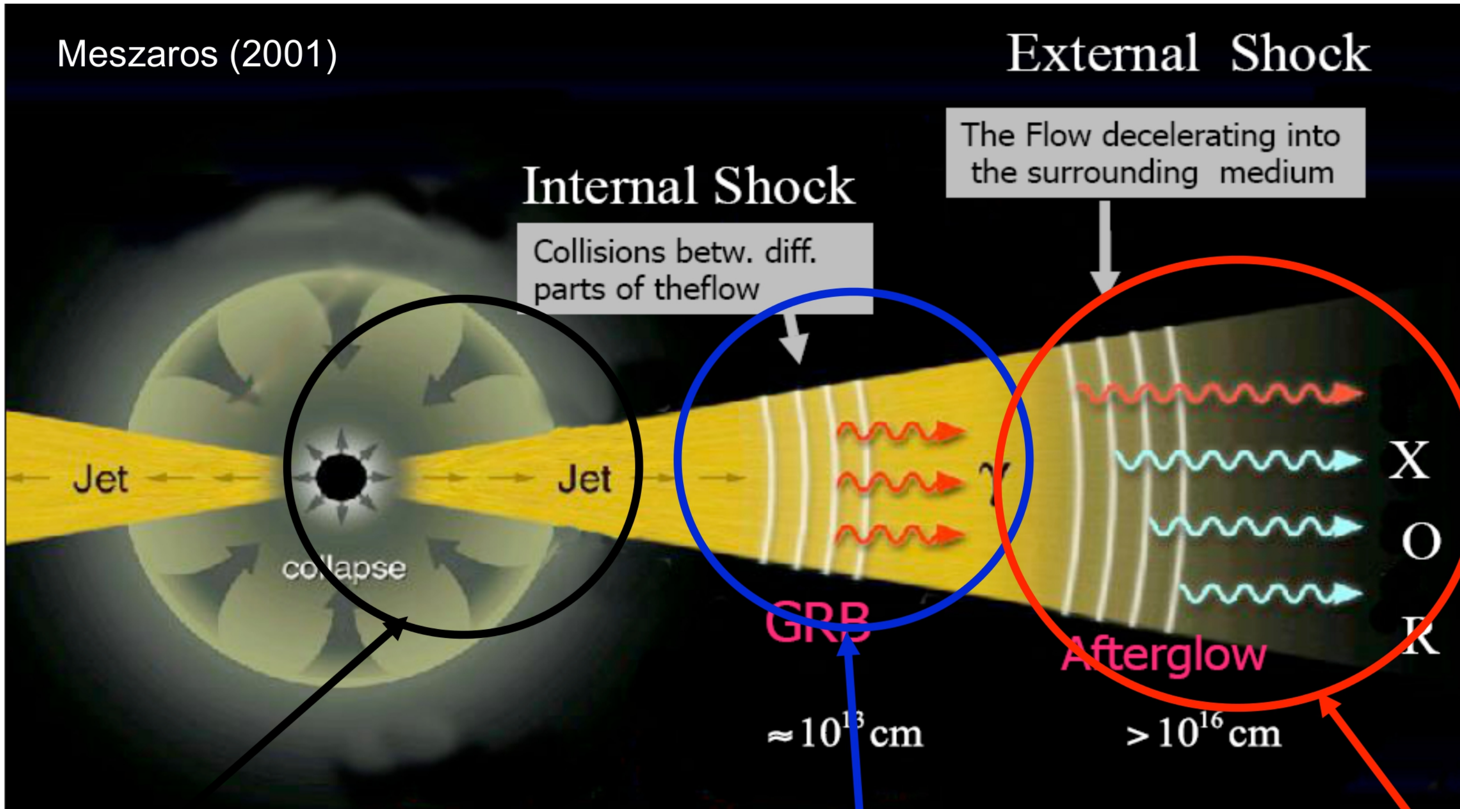

Inner jet inside a star
$r < 10^{12}$ cm, $B > 10^6$ G
TeV-PeV ν, no γ
Meszaros & Waxman 01 PRL
Razzaque et al. 03 PRL
KM & Ioka 13 PRL

Inner jet (prompt/flare)
$r \sim 10^{12}$-10^{16} cm $B \sim 10^{2\text{-}6}$ G
PeV ν, GeV-TeV γ
Waxman & Bahcall 97 PRL
Dermer & Atoyan 03 PRL
KM & Nagataki 06 PRL

Afterglow
$r \sim 10^{14}$-10^{17} cm $B \sim 0.1$-100 G
EeV ν, GeV-TeV γ
e.g., Waxman & Bahcall 00 ApJ
Dermer 02 ApJ
KM 07 PRD

Photohadronic production of neutrinos

Basic approach by Waxman and Bahcall: approximation of $p\gamma$ interaction cross section using **$\boldsymbol{\Delta}$-resonance**

$$p + \gamma \to \Delta^+ \to \begin{cases} n + \pi^+ & \text{1/3 of all cases} \\ p + \pi^0 & \text{2/3 of all cases} \end{cases}$$

The π^+ **decay** producing ν_μ, $\bar{\nu}_\mu$ and ν_e in the process

$$\begin{aligned} \pi^+ \quad &\to \quad \mu^+ + \nu_\mu \\ & \qquad \mu^+ \to e^+ + \nu_e + \bar{\nu}_\mu \end{aligned}$$

Standard conclusion

ν result from interaction of p and γ in GRBs, with a ratio $(\nu_e : \nu_\mu : \nu_\tau)$ of $(1:2:0)$, or $(1:1:1)$ after flavor mixing.

See e.g. [Waxman and Bahcall, Phys. Rev. Lett. **78** (12), 2292 (1997)]

Constraints from IceCube for prompt GRB ν flux

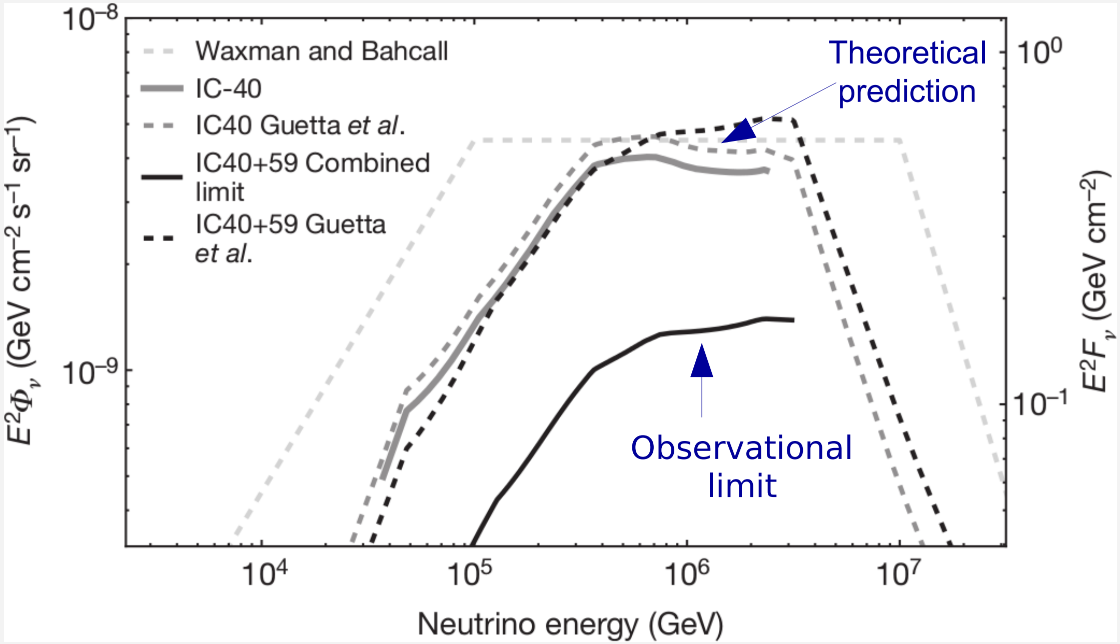

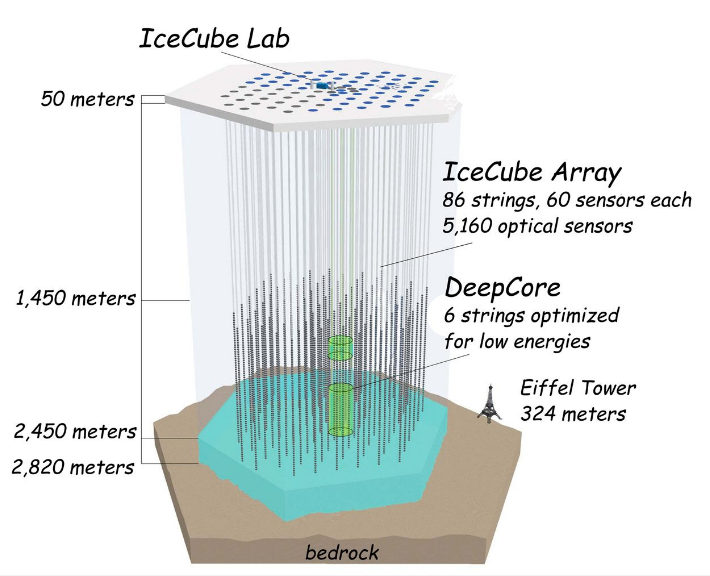

Comparison of predictions of flux from GRBs based on observed gamma-ray spectra (dashed lines) with 90% condence upper limits obtained from the results of IceCube for 40 and 59 detector strings (Abbasi et al. 2012).

- The efficiency of neutrino production may be much lower than what has been predicted (Abbasi et al. 2012).
- Constraints for a prompt neutrino flux from GRBs were derived from 4-years IceCube data. A single low-significance neutrino, compatible with the atmospheric neutrino background, was found in coincidence with one of the 506 observed GRBs (Aarsten et al. 2015).
- Coincidence analysis between Fermi / LAT gamma-ray data and IceCube neutrino data did not reveal significant coincidence (Turley et al. 2018).

Future mission CAMELOT for Localisation of Gamma-Ray Transients by Fleet of Cubesats

Jakub Řípa
Charles University, Astronomical Institute
MTA-Eötvos Loránd University

Norbert Werner, Andras Pál, Norbert Tarcai, Gábor Galgóczi, Zsolt Várhegyi, Zsolt Frei, László Kiss

Masanori Ohno, Yasushi Fukazawa, Tsunefumi Mizuno, Hiromitsu Takahashi, Koji Tanaka, Nagomi Uchida, Kento Torigoe, Kazuhiro Nakazawa, Teruaki Enoto, Hirokazu Odaka, Yuto Ichinohe

SZÉCHENYI 2020
HUNGARIAN GOVERNMENT
European Union
European Social Fund
INVESTING IN YOUR FUTURE

広島大学
名古屋大学 NAGOYA UNIVERSITY

17. 08. 2017 BEGINNING OF MULTI-MESSENGER ASTROPHYSICS OF GRBs

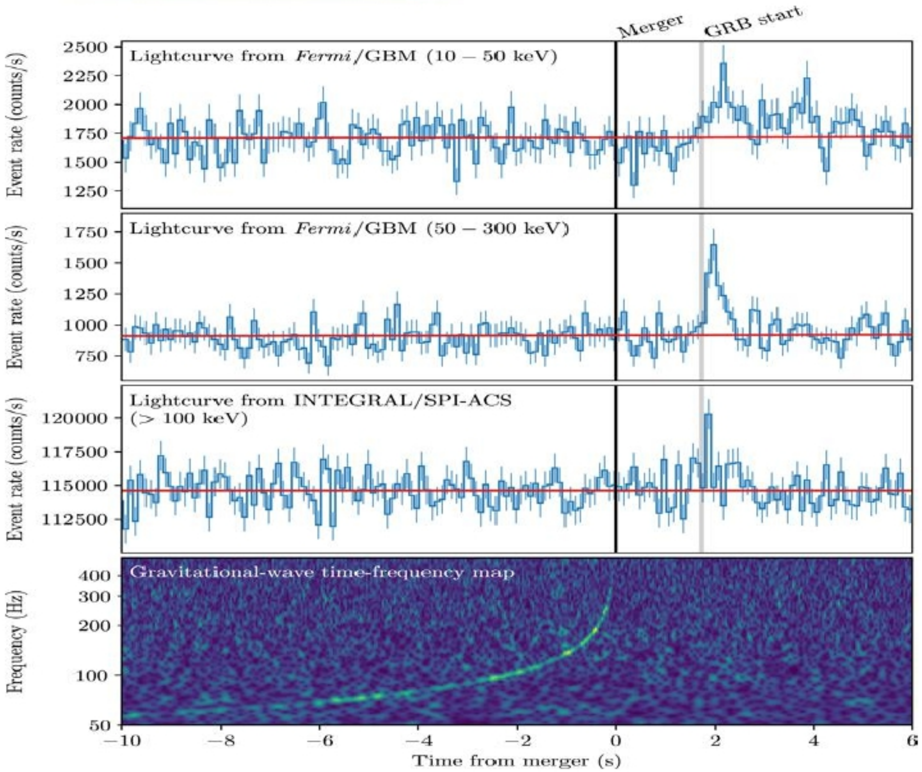

- 5 gravitational wave detections from BH-BH merger
- EM counterpart from NS-NS merger event GW170817/GRB170817A
- Large campaign of follow-up observations identified a kilonova
- The gamma-ray counterpart is unusual
- **Regular detections/follow-up observations are needed to make progress**

AN EMPTY REGION IN PARAMETER SPACE

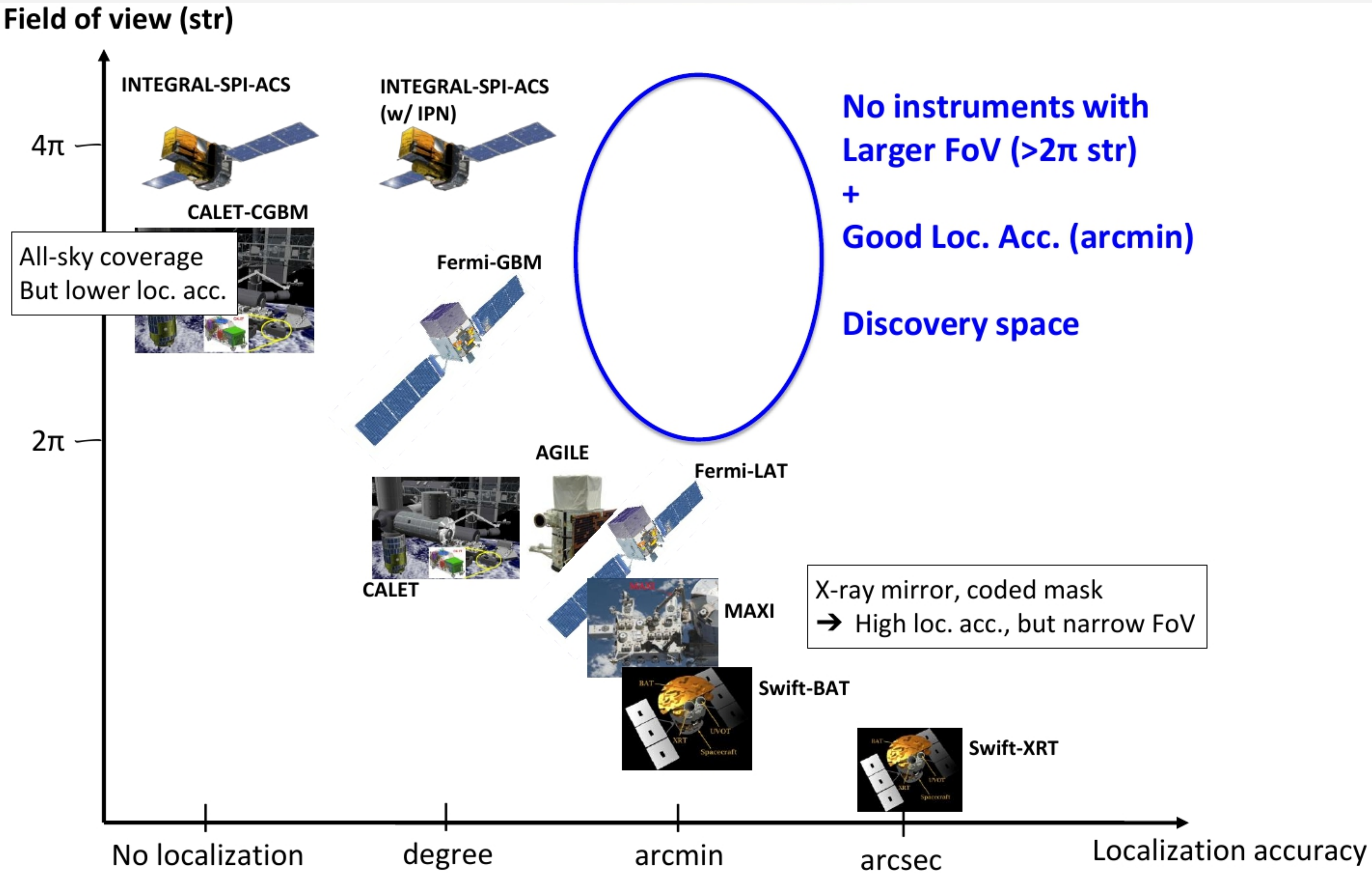

CAMELOT: Cubesats Applied for MEasuring and LOcalising Transients

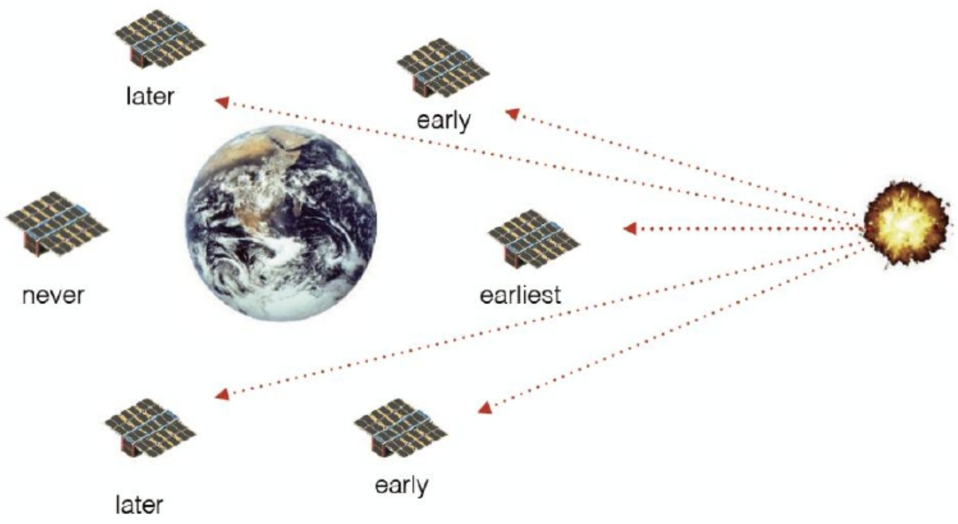

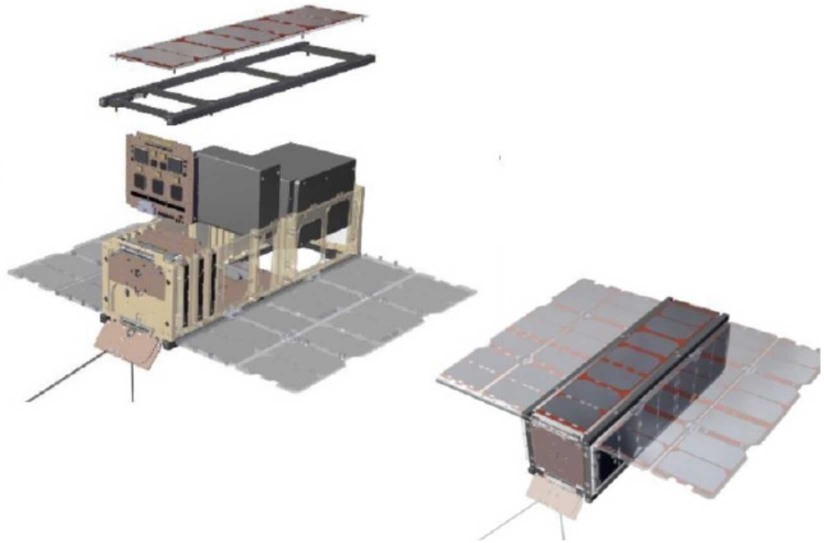

A constellation of at least 9 satellites can provide:

- all sky coverage with a large effective area
- Better than 0.1 millisecond timing accuracy
- ~10 arcmin localisation accuracy using triangulation

Each satellite will use a standard 3U cubesat platform developed by C3S LLC for the ESA sponsored RadCube mission. The cubsesats will be equipped with a *GPS receiver for precise time synchronisation* and *inter-satellite* (Iridium NEXT) *communication* equipment for *rapid data download*

TWO POSSIBLE DETECTOR CONFIGURATIONS

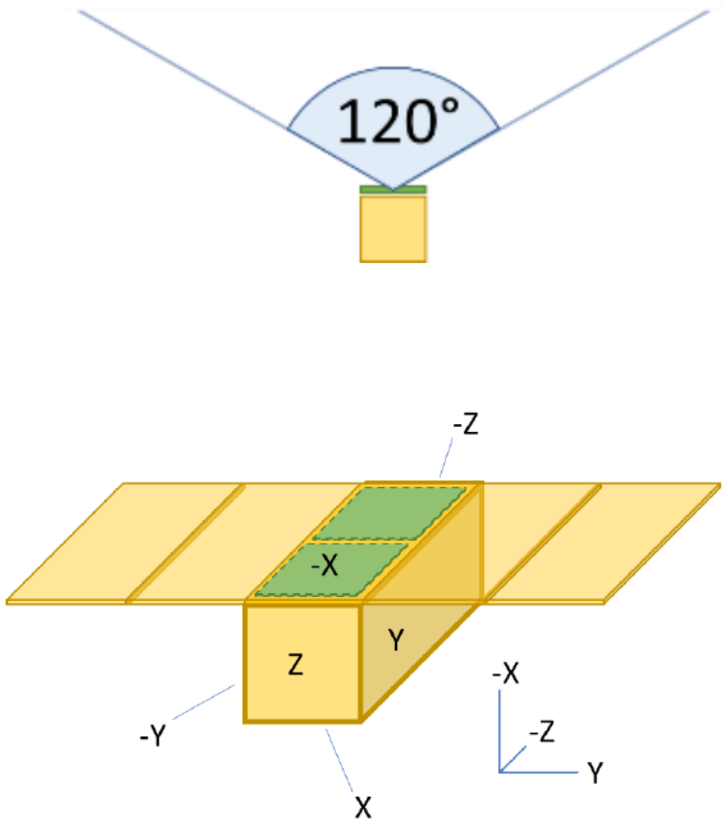

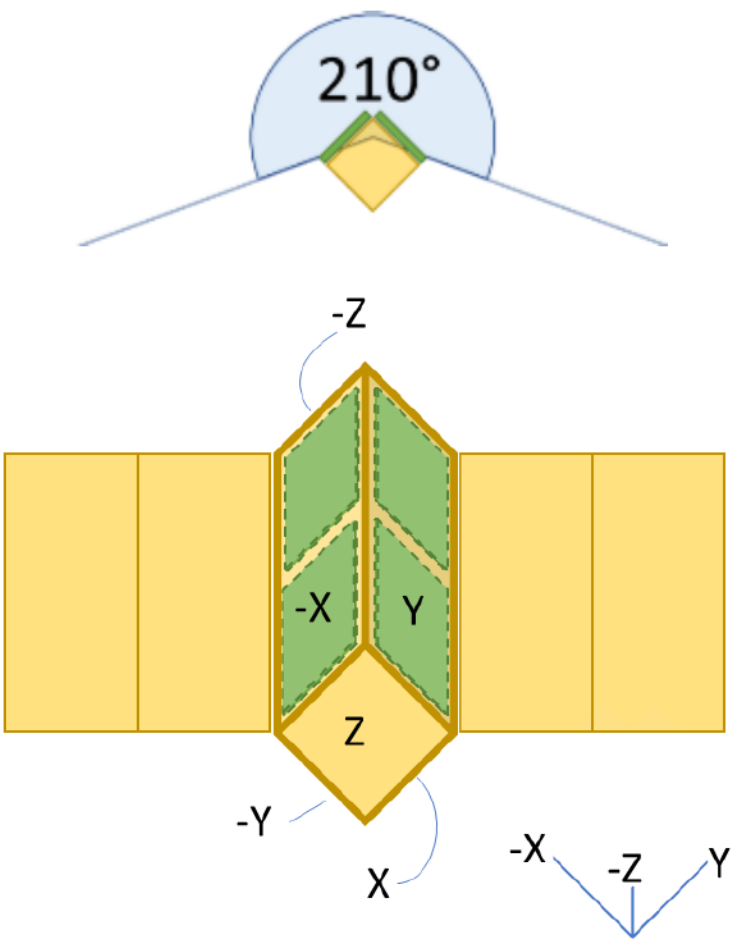

THE DETECTOR DESIGN

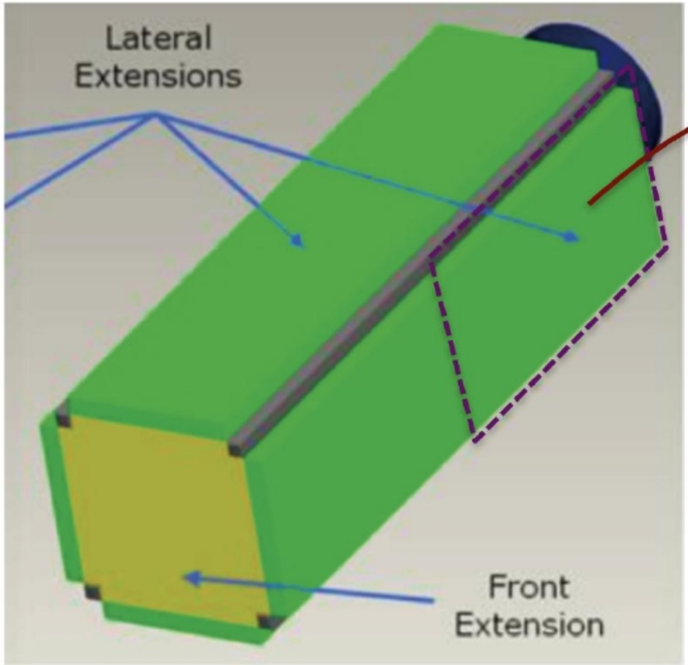

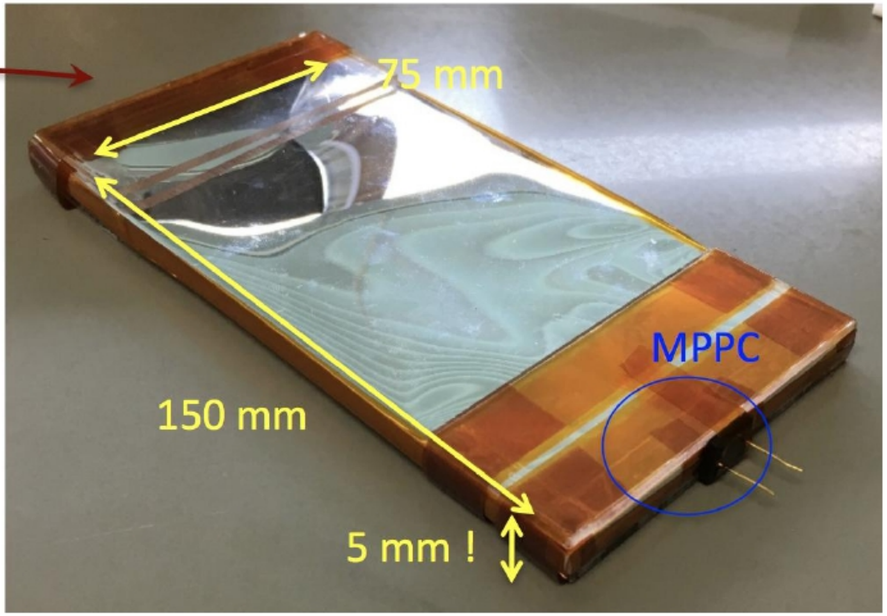

To maximise the effective area, the detectors based on CsI scintillators and Multi-Pixel Photon Counters (MPPC) will occupy two lateral extensions (8.3 cm x 15 cm x 0.9 cm x 4)

The large and thin detectors with small readout area are challenging

The read out of the CsI detectors with MPPC is currently being evaluated in the lab as part of our feasibility study. The system provides a large light yield, compact readout area and relatively low operational voltage.

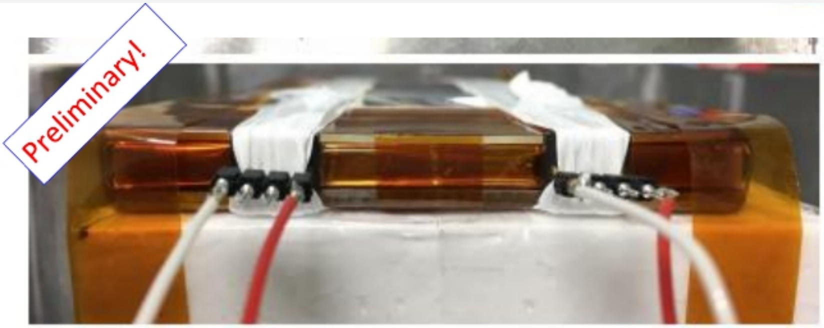

Torigoe+ 2018

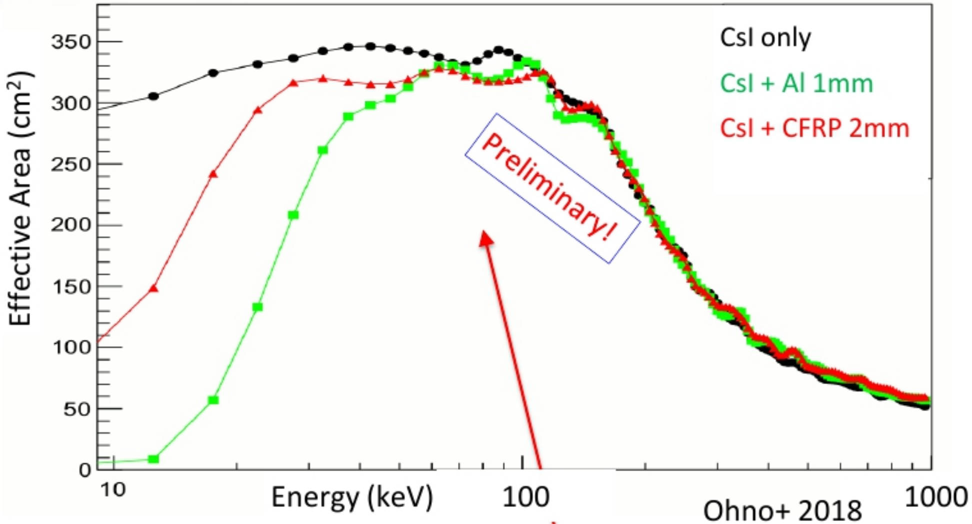

Ohno+ 2018

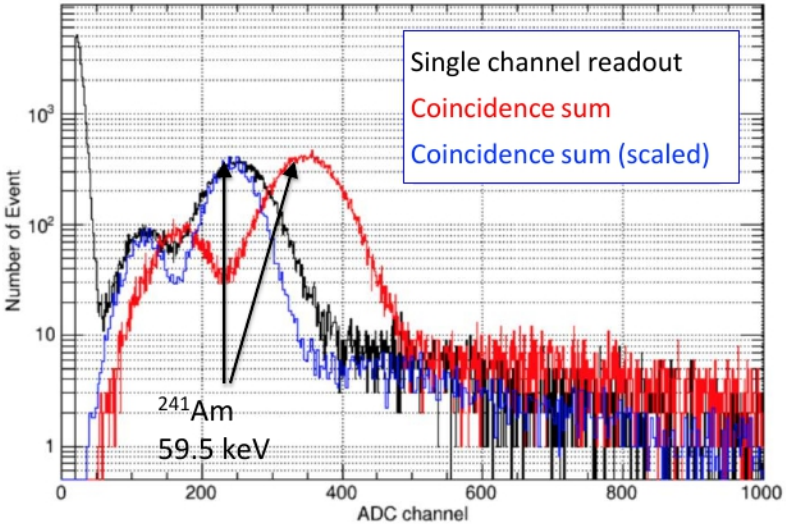

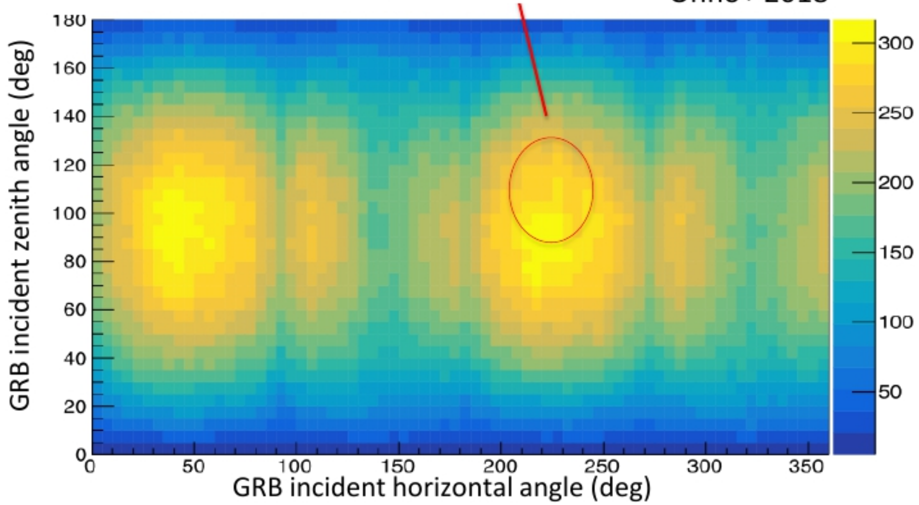

Energy threshold of ~10 keV is achieved for both single/multi channel readout
Energy range: 10-1000 keV (TBD)

Effective area for best incident angle is estimated by the Monte-Carlo simulation, ~300 cm² (@100 keV)

Effective area of one satellite is comparable to two Fermi-GBM detector modules

CAMELOT GPS TIME-STAMPING TEST BOARD

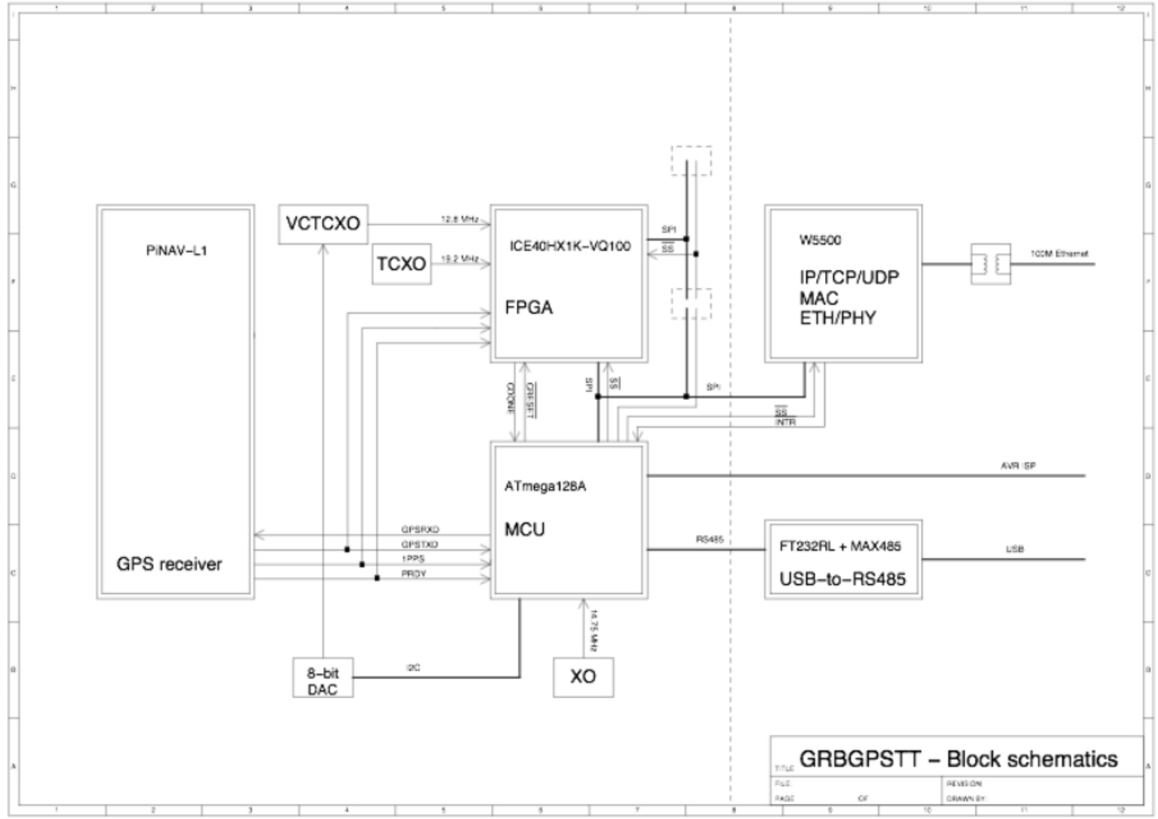

Pál et al. 2018

SKY VISIBILITY ON 53 DEG WALKER ORBITS

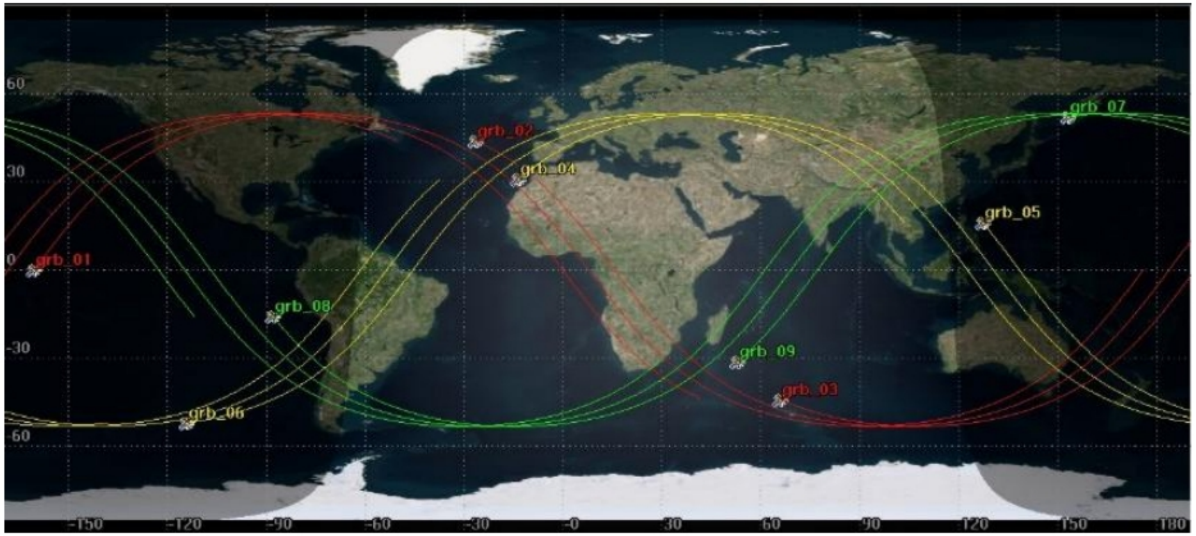

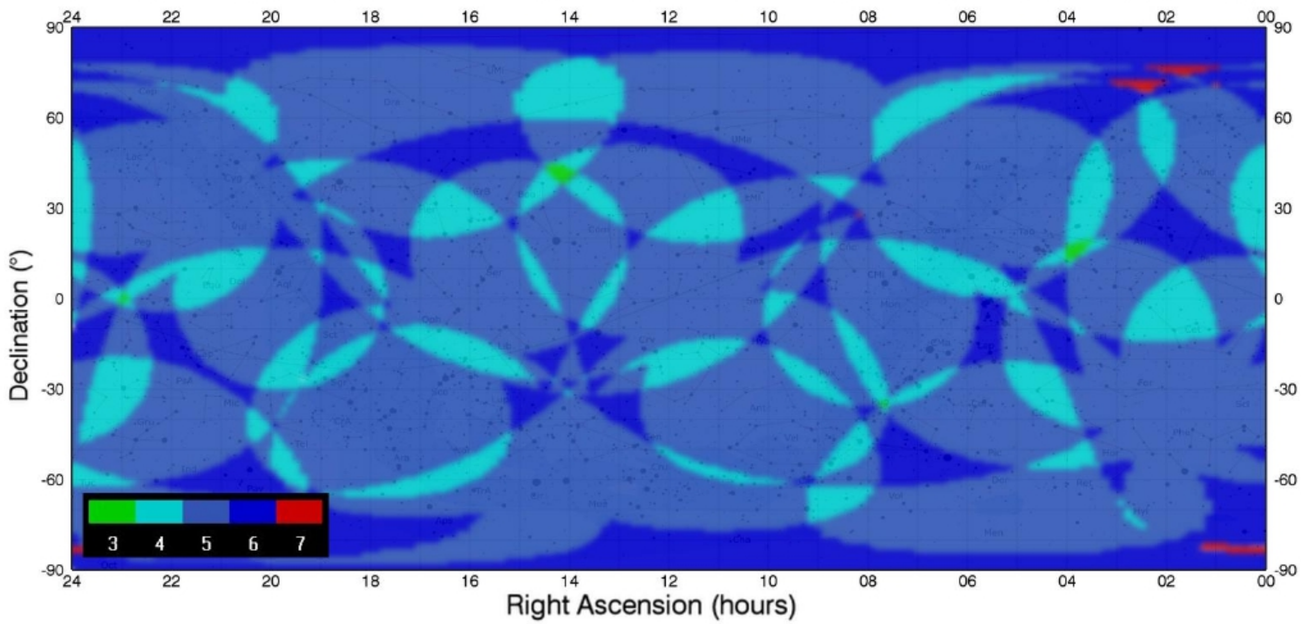

95% of the sky will be simultaneously covered by at least 5 satellites.

SKY VISIBILITY ON SUN-SYNCHRONOUS POLAR ORBITS

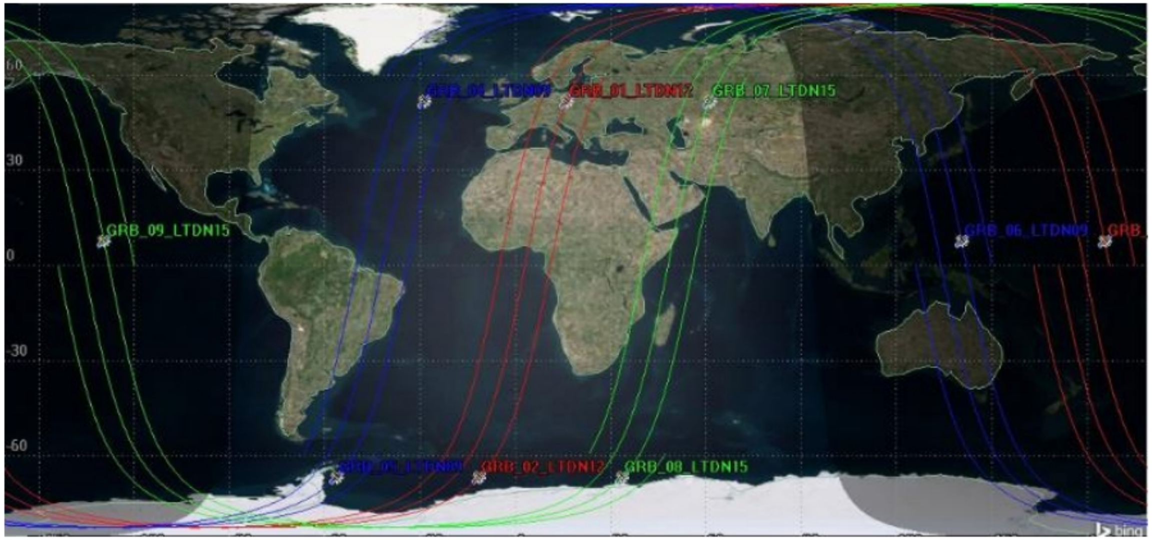

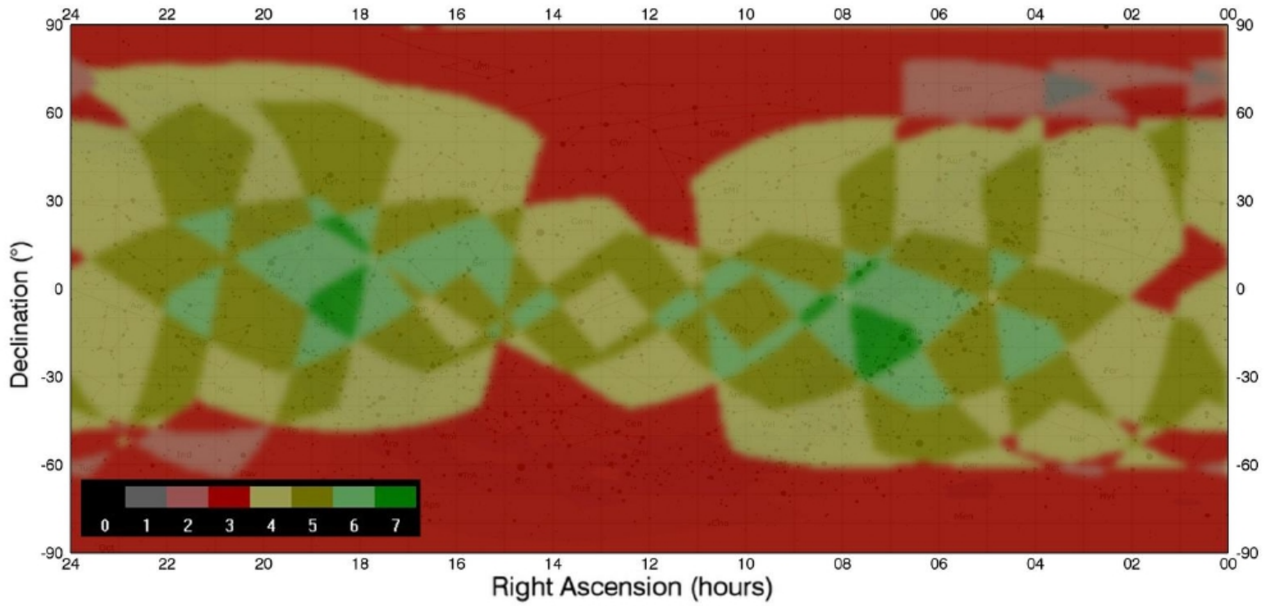

HIGH BACKGROUND ON POLAR ORBITS

Electron flux by ESA-SEE1 model at 500 km

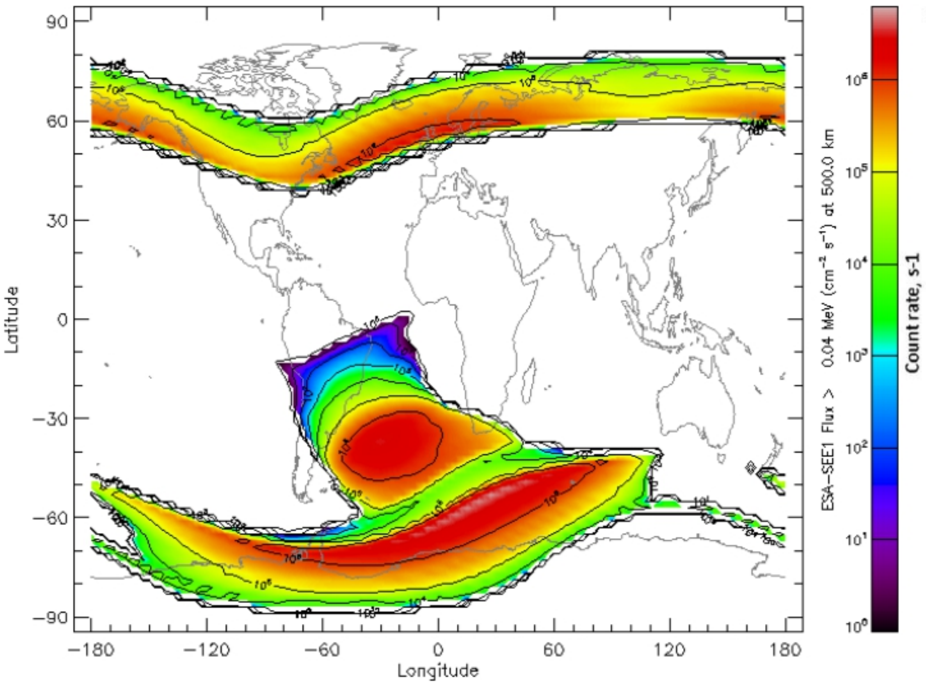

Lomonosov / BDRG count rate in scintillator-based GRB detector on polar orbit (~500 km).

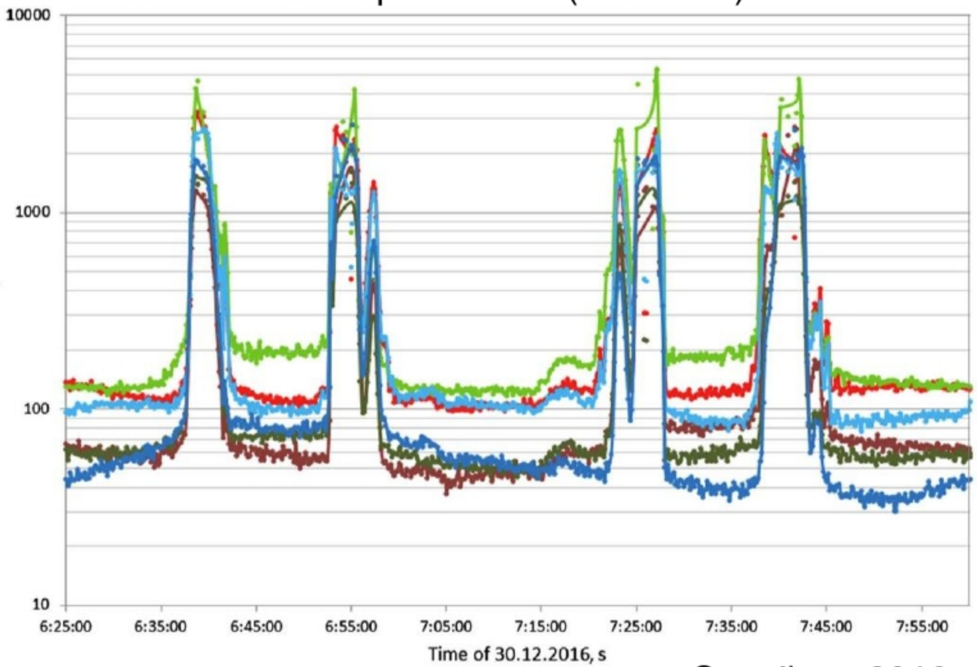

Svertilov+ 2018

On **polar** orbit, each satellite will **loose ~30-40%** of observing time.

On **53° inclination** orbit, each satellite will **loose ~20%** of observing time.

WHAT DO WE EXPECT TO SEE?

- Over **300 GRBs** detected per **year**
- Many **terrestrial gamma ray flashes**, solar flares, soft gamma ray repeaters, X-ray binaries, etc.

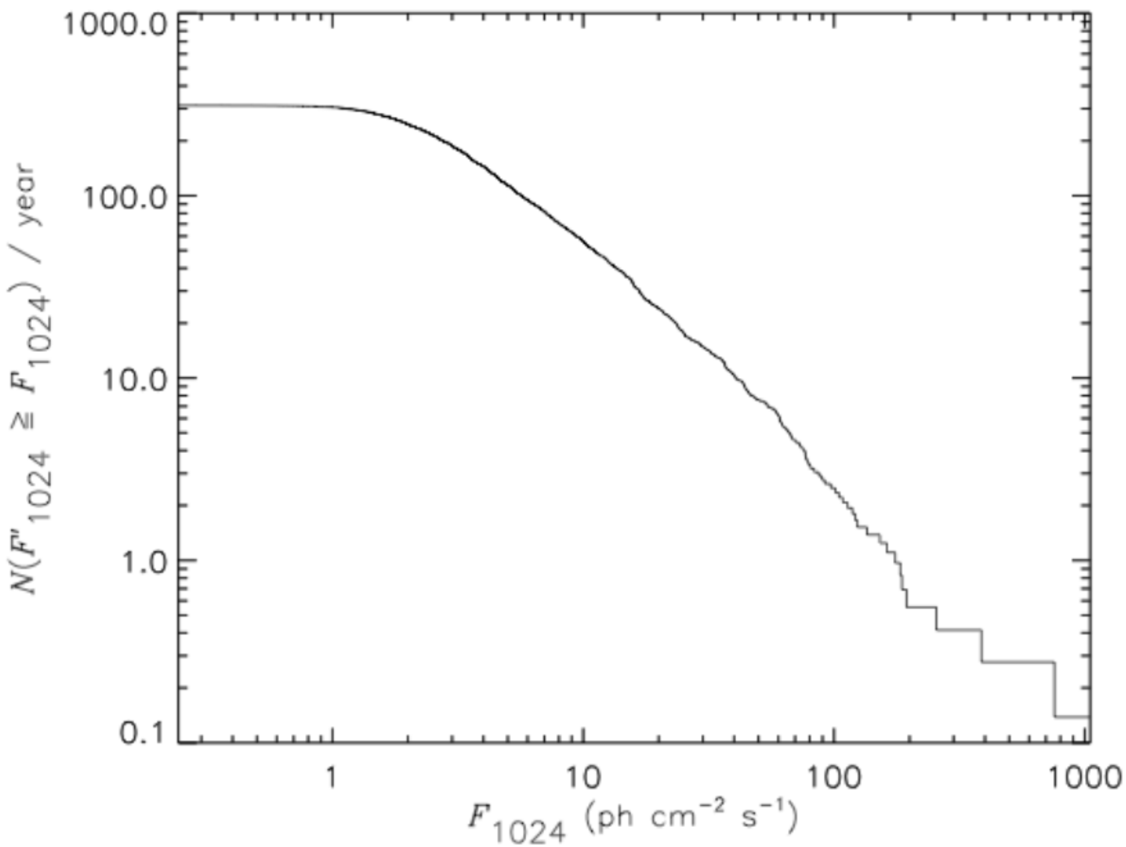

TIMING BASED LOCALISATION

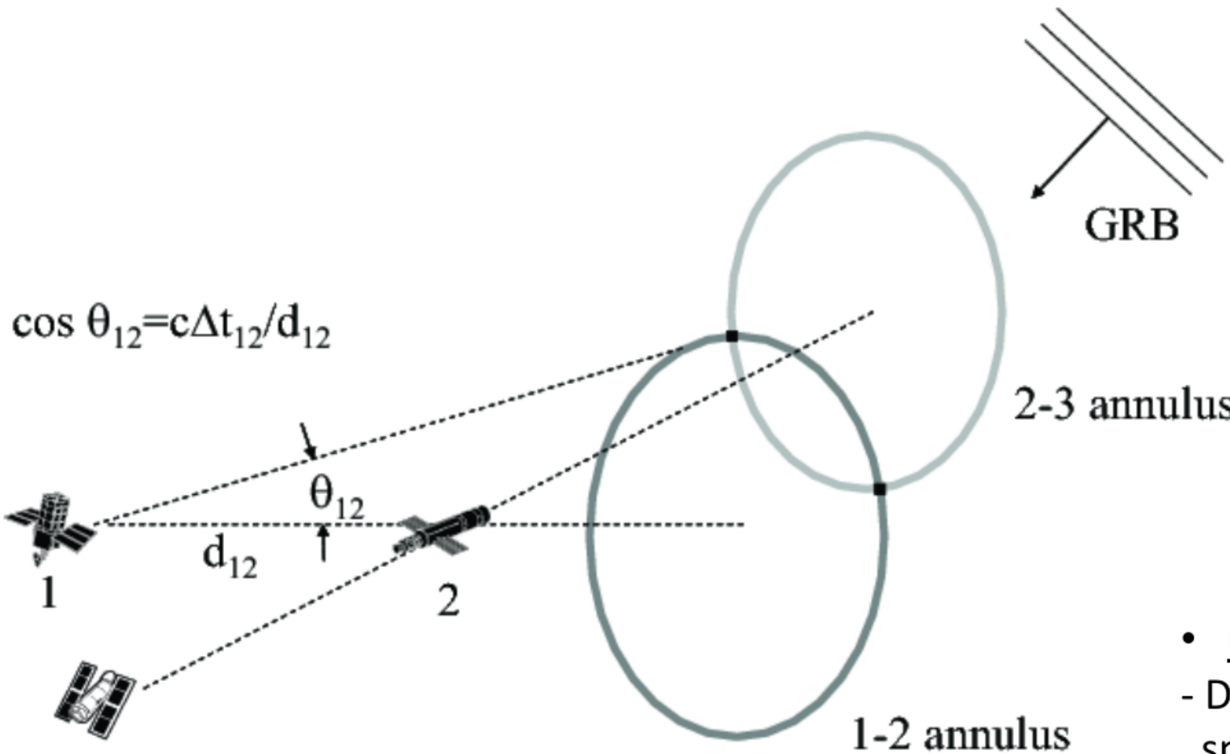

Hurley+13

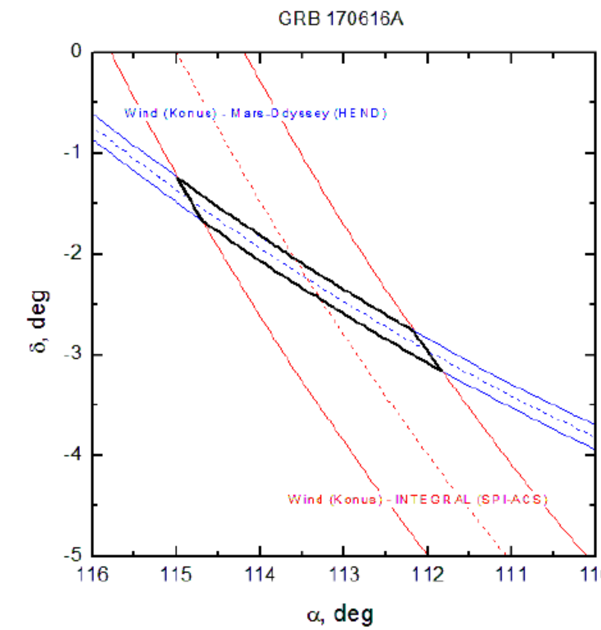

- IPN deals with:

- Different clock accuracy from one spacecraft to another
- Various time resolutions
- Uncertainty in s/c positions for far-Earth s/c
- Different energy responses of various detectors

- localisation by photon arrival time

High timing synchronization by GPS + 10μ-sec absolute timing accuracy results several arcmin localisation accuracy ?

LOCALISATION FEASIBILITY

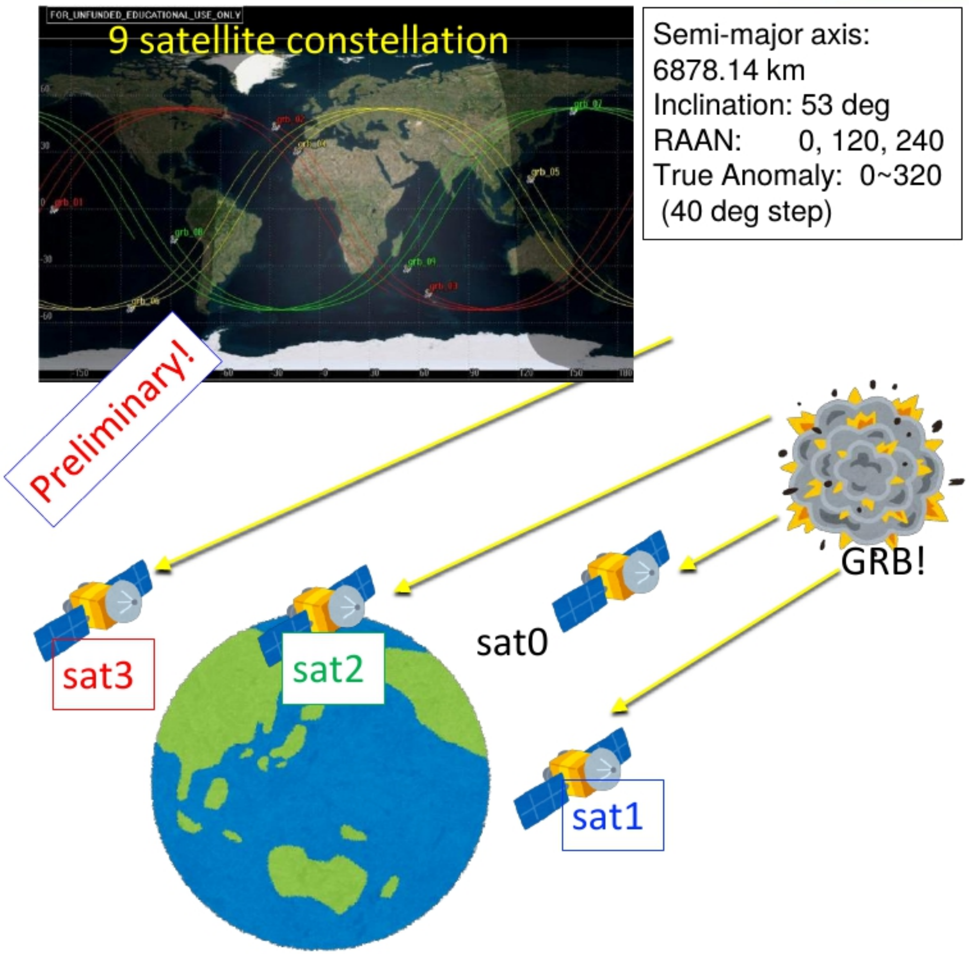

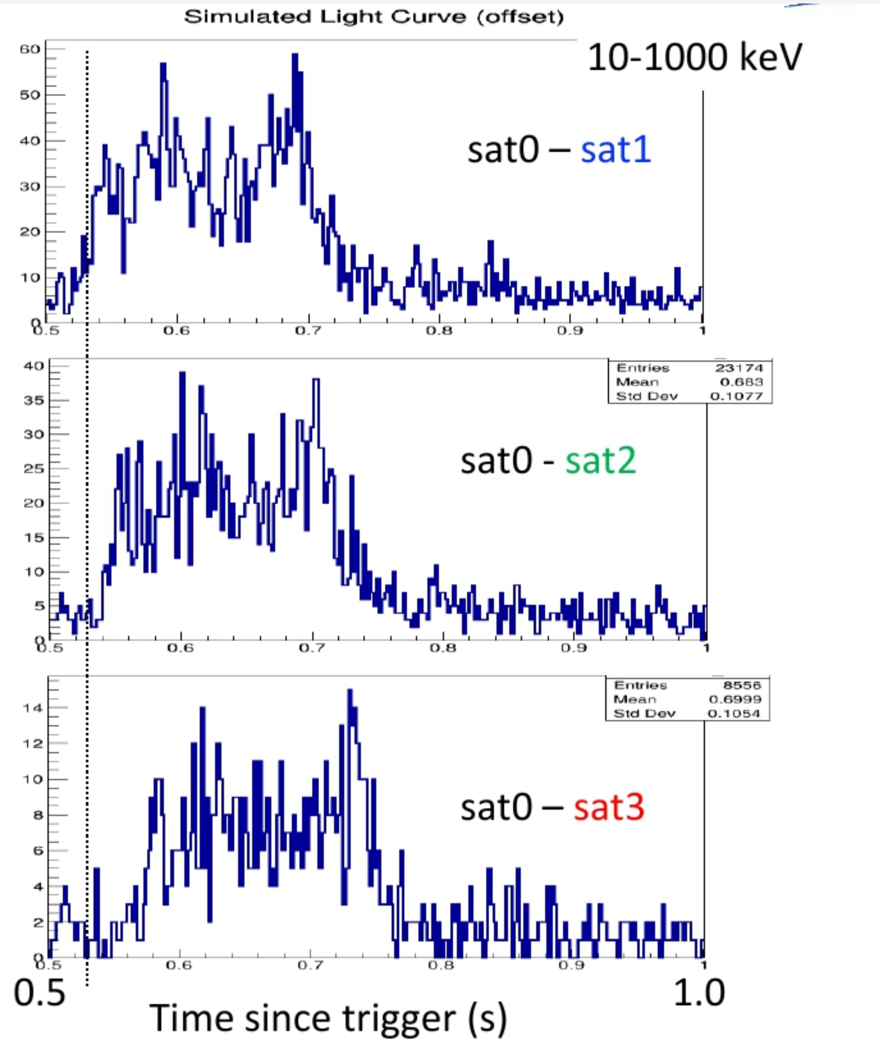

Satellite attitude, GRB position, predicted photon count/arrival time estimated using orbit and detector simulations.

Simulated photon arrival time is estimated by the cross correlation analysis ➔ triangulation annulus

Ohno et al. 2018

Intersection of annuli

➔ GRB position!

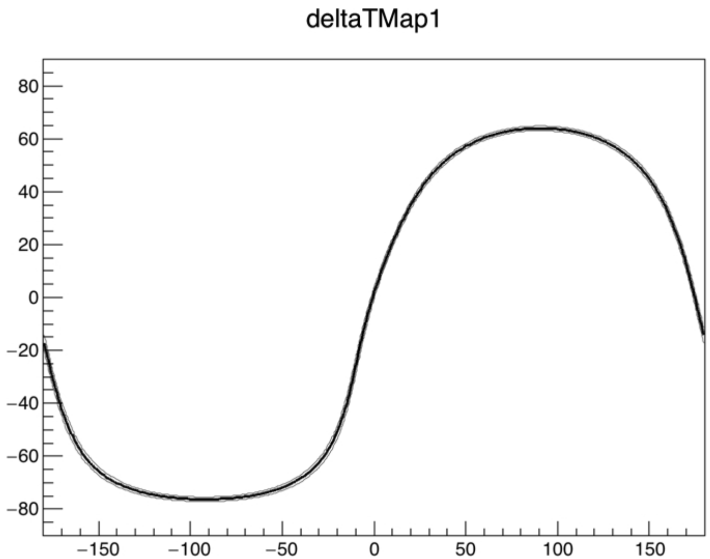

How can we estimate the most probable position and error ?

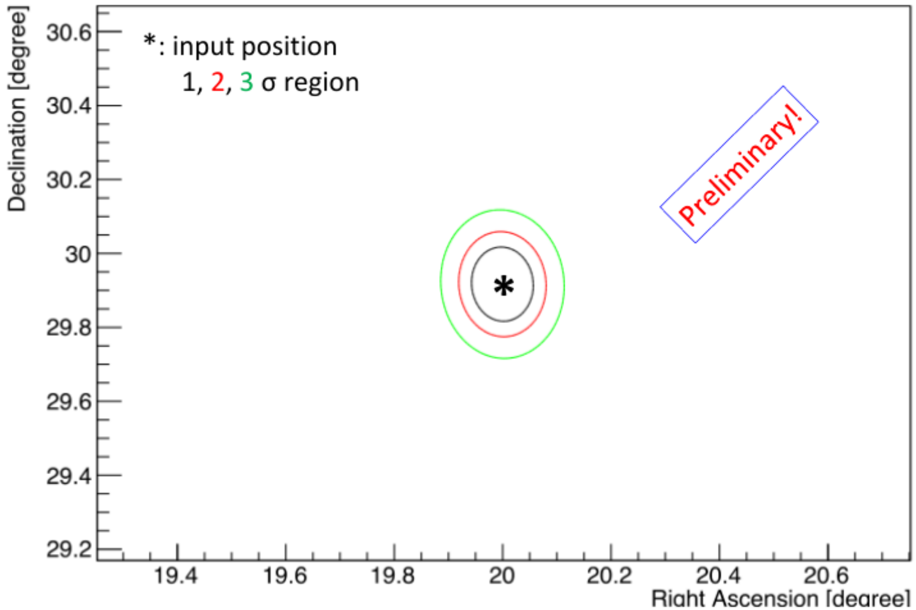

$$\chi^2 \equiv \sum_{i=0}^{N} \frac{\left\{\delta t_{\rm sim,i} - {\rm Norm} \times \cos\theta_{\rm model,i}({\rm R.A.}, {\rm Dec.}) \times {\rm D/c}\right\}^2}{\sigma^2_{\rm sim,i}},$$

GRB position and error is estimated by simple χ^2 minimization (Tanaka+ 17)

~0.1 $\deg_{1\sigma}$ (~6 arcmin) accuracy is achievable for bright/high-visibility case

Best fit position
R.A. = 20.0 (+/- 0.06) deg
Dec. = 29.9 (+/-0.10) deg

Ohno et al. 2018

LOCALISATION ACCURACY

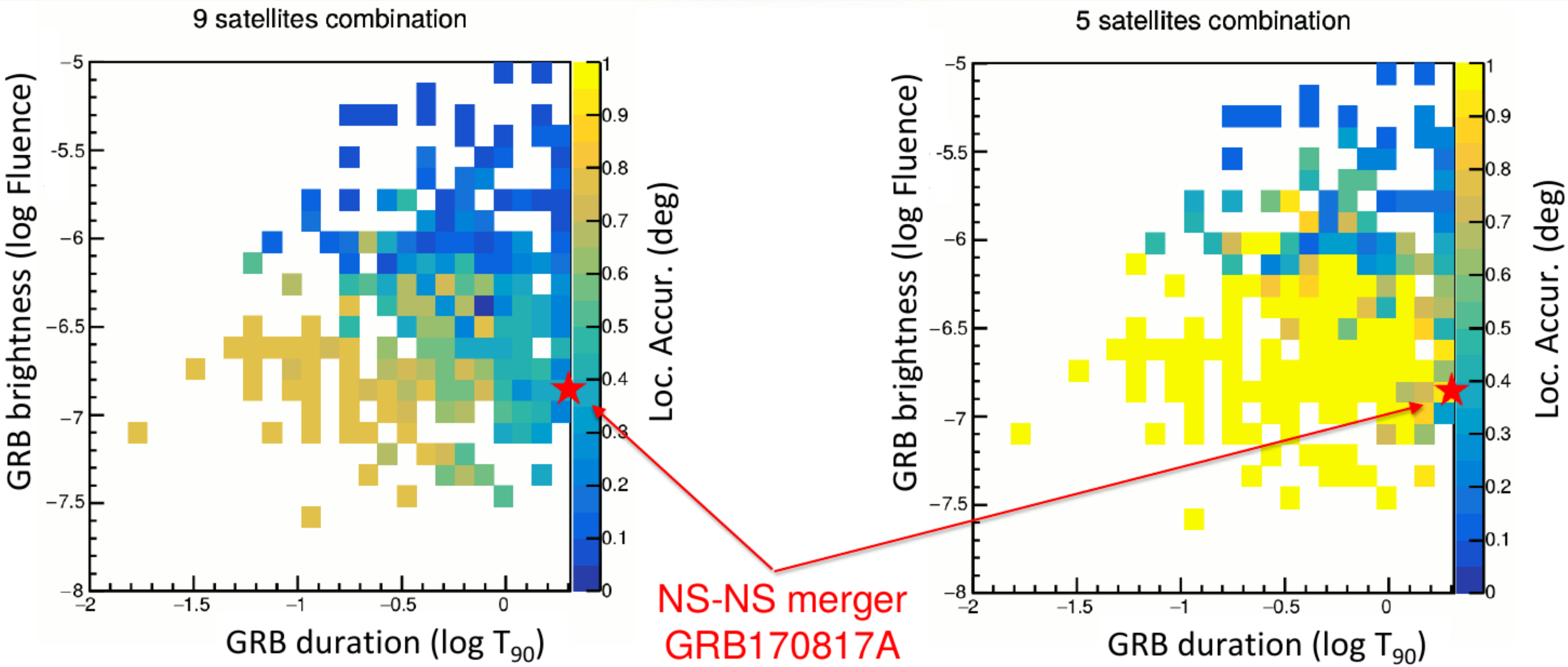

Localization accuracy of our concept is examined for all short GRBs listed in Fermi 3rd GRB Catalog (Bhar+16 T_{90}<2s: 326 events)

- **High localisation accuracy for good photon statistics (brighter/longer)**
- **5-10 arcmin accuracy in the best case**
- **Ten short GRBs per year localised to within 20 arcmin**

Ohno et al. 2018

Tests of Lorentz Invariance Violation

Tests of Lorentz Invariance Violation

- Lorentz invariance: the laws of physics in a non-accelerated system are not affected when this system undergoes Lorentz transformation. For example the speed of light is constant and does not depend on the reference system. However, many Quantum Gravity theories have suggested that the propagation of light through the space-time with a foamy structure would show a dispersion relation in vacuum (Amelino-Camelia et al. 1998), speed of light would depend on energy, which could lead to the violation of Lorentz invariance (LIV).
- See: Abbott et al. 2017; Abdo et al. 2009; Bernardini et al. 2017; Boggs 2004; Ellis et al. 2006; Ellis et al. 2018; Martinez and Piran 2006; Petitjean et. al 2016; Wei et al. 2017; Wei et al. 2017; Zhang and Ma 2015.

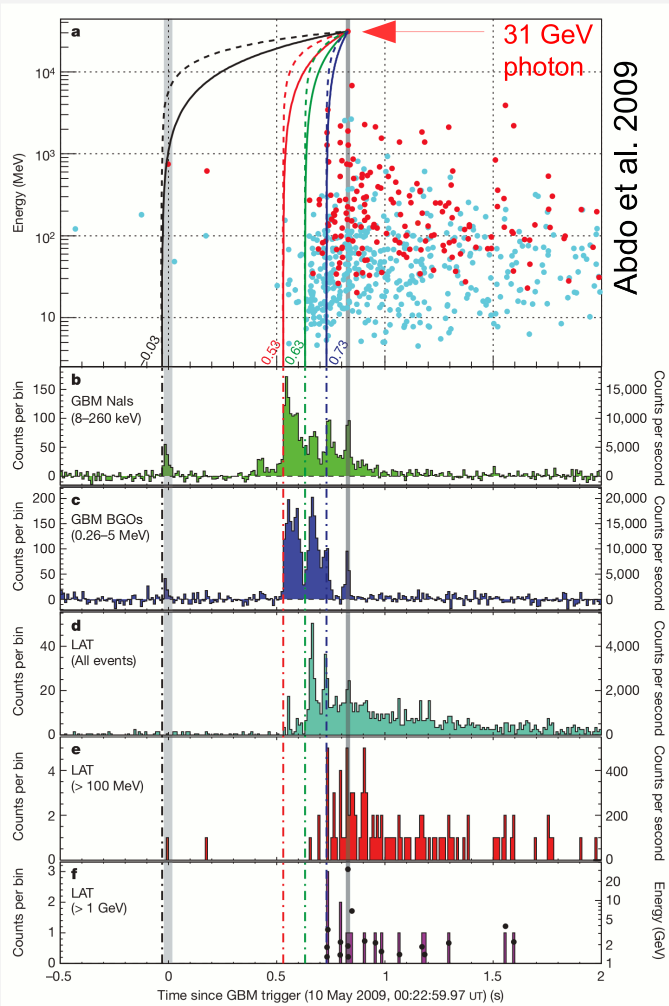

- Some quantum-gravity theories predict the photon-propagation speed v_{ph} varying with photon energy E_{ph}. At energies $E_{ph} << E_{Planck}$ (1.22×10^{19}GeV) the $|v_{ph}/c - 1| \approx (E_{ph}/M_{QG,n}c^2)^n$, where M_{QG} is the quantum gravity energy scale for order n and n=1 or 2 is usually assumed and $c \equiv v_{ph}(E_{ph} \rightarrow 0)$.
- Abdo et al. 2009 found no evidence for the violation of Lorentz invariance for GRB 090510 at z=0.9.

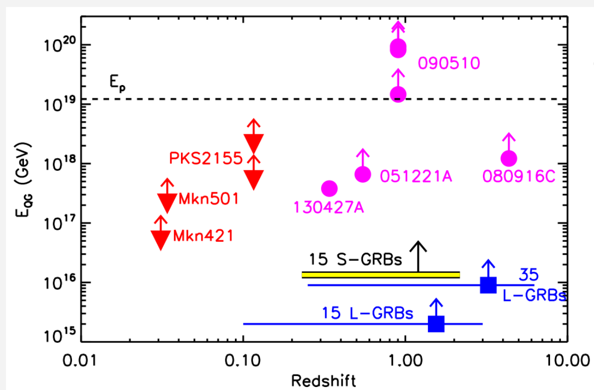

Fig. 1. Current limits on the quantum gravity energy scale available in the literature from extragalactic sources: TeV blazars (red triangles: Mkn 421, Biller et al. 1999; Mkn 501, MAGIC Collaboration et al. 2008; PKS 2155-304, Aharonian et al. 2008; H.E.S.S. Collaboration et al. 2011), single GRBs (magenta points: S-GRB 051221A, Rodríguez Martínez et al. 2006; L-GRB 080916C, Abdo et al. 2009b; S-GRB 090510, Abdo et al. 2009a; Ghirlanda et al. 2010; Vasileiou et al. 2013; L-GRB 130427A, Amelino-Camelia et al. 2013) and samples of L-GRBs (blue squares, Bolmont et al. 2008; Ellis et al. 2008), compared to the result obtained in the present work.

- However, the physical origin of the intrinsic spectral lag of GRB prompt gamma light curves is still unclear, and it is not possible to predict theoretically its value for specific events, thus it is hard to disentangle its contribution from the purely quantum-gravity delay of photons.

Bernardini et al. 2017

Review: GRBs In a Nutshell

GRBs In a Nutshell

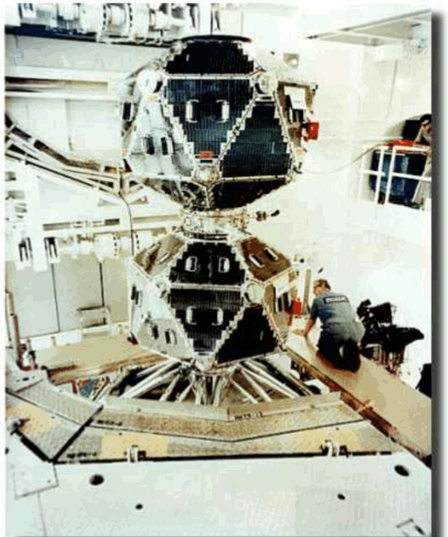

Discovered by VELA satellites in late 60's

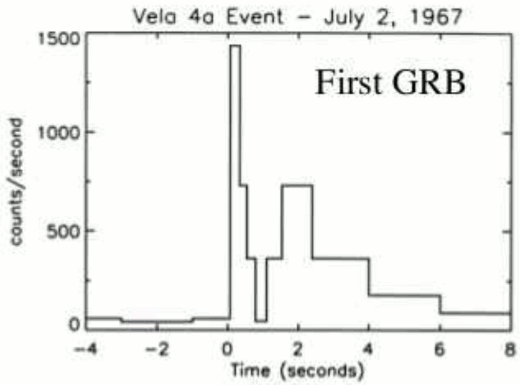

Klebesadel, Strong & Olson 1973

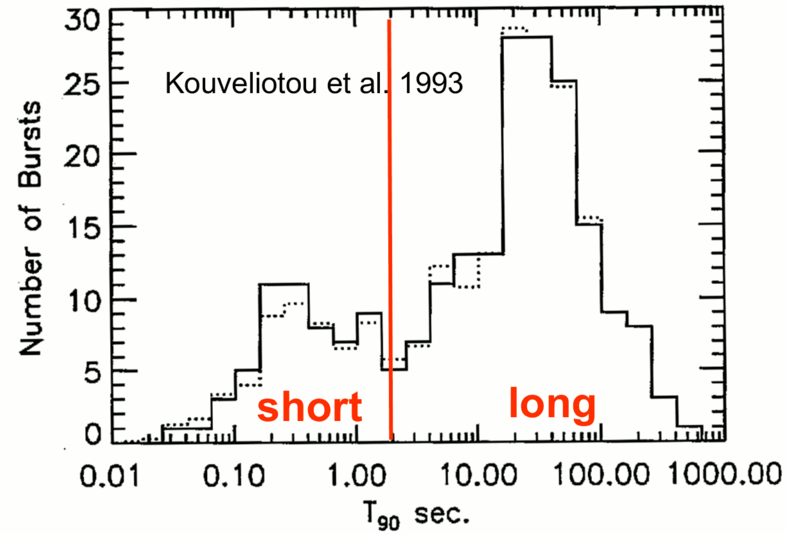

Fishman et al. 1994,
BATSE instrument

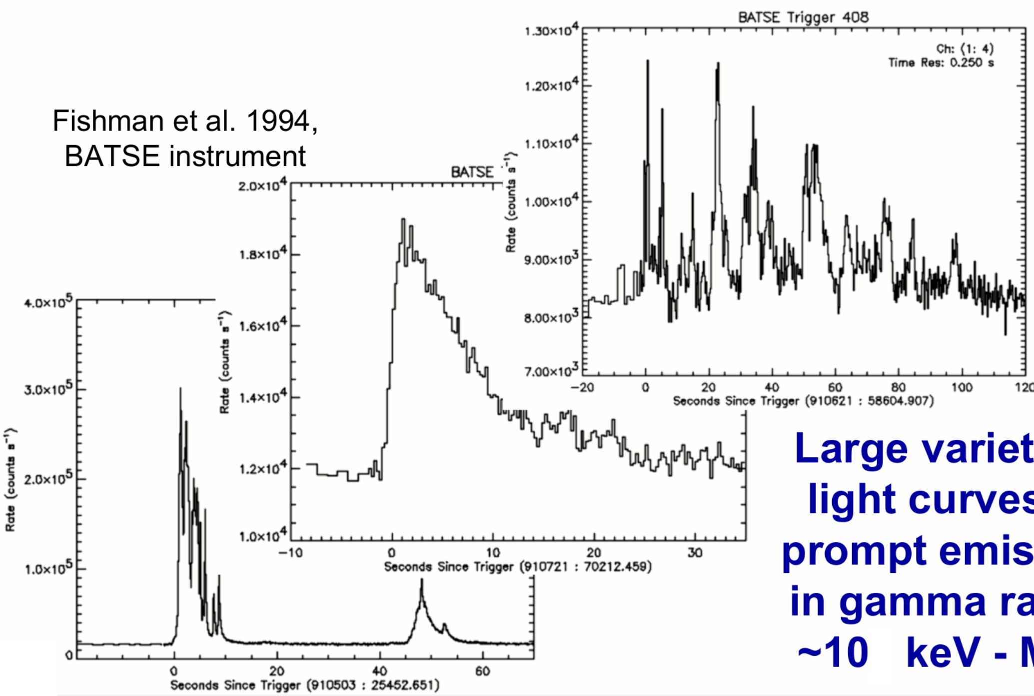

Large variety of light curves of prompt emission in gamma range ~10 keV - MeV

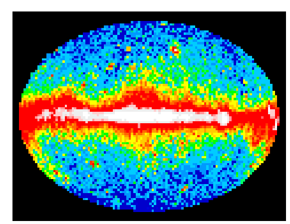

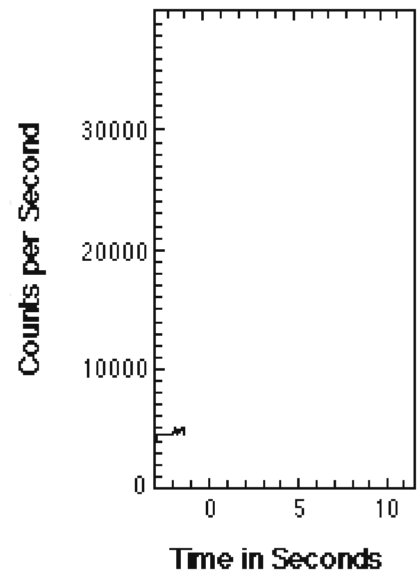

GRBs In a Nutshell

Upper plot:

- Photon number flux N_E:

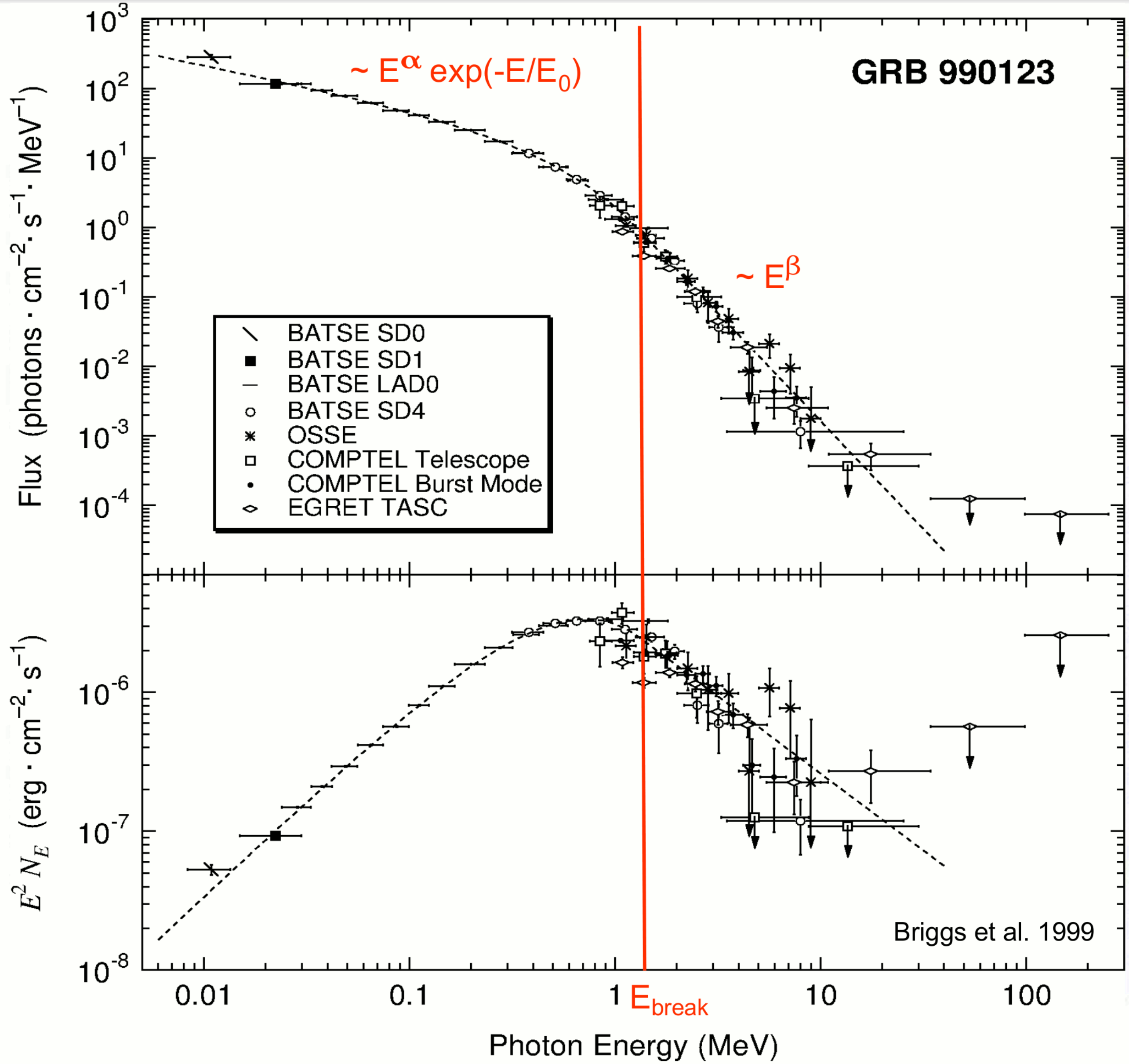

- Energy flux $E^2 \times N_E$
- allows easy comparison of source luminosities in different wavelength bands.
- GRB luminosity maximal at E_P

Time integrated prompt spectrum of GRB990123 observed by CGRO.
Dashed line is fitted Band function with parameters $\alpha = -0.6$, $\beta = -3.1$ and $E_p = 720$keV.

GRBs In a Nutshell

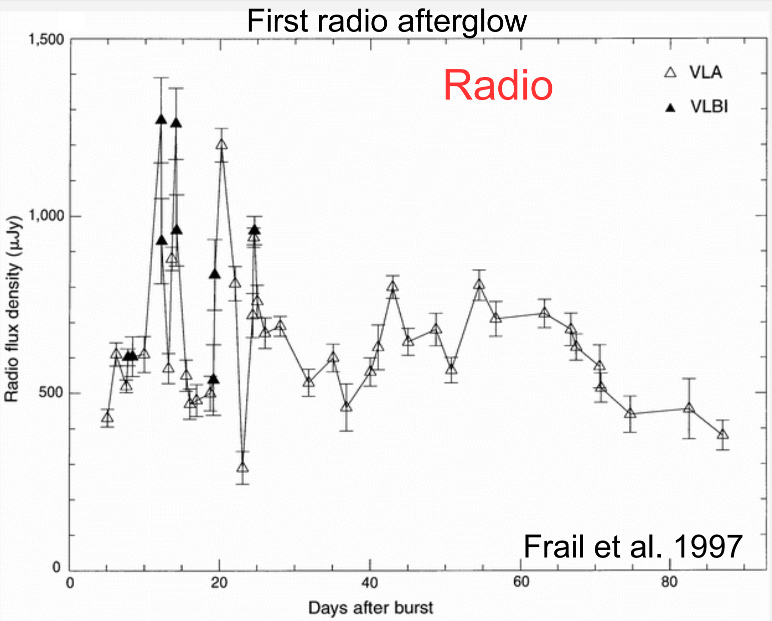

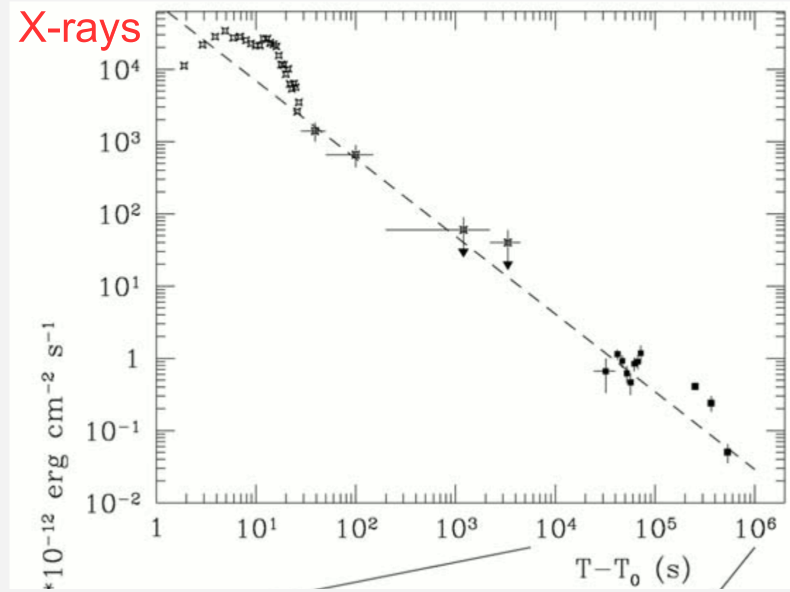

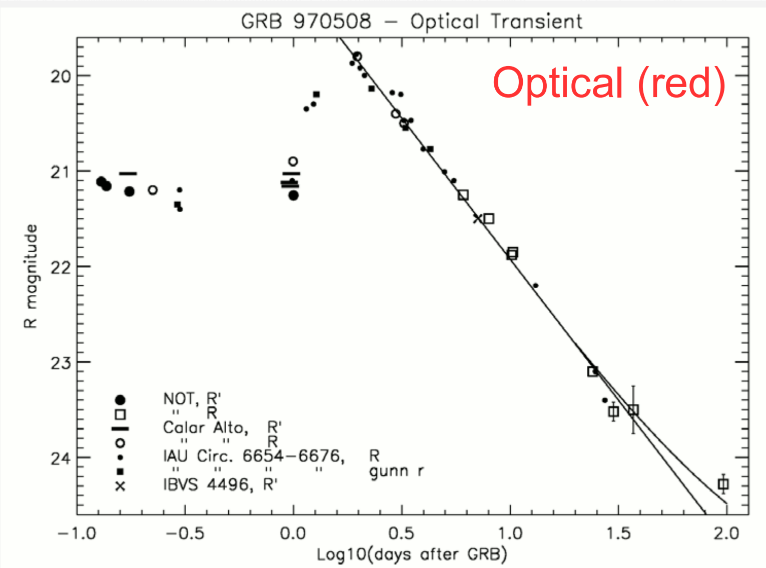

R-band light-curve of the optical transient associated with GRB 970508. Following a period of modest decline, a peak of optical emission was reached about 40 h after the GRB. After this peak, the emission declines following a power law ($F \propto t^{-1.21}$). A possible contribution of a constant source, the host galaxy with R-magnitude of 25.5 is shown by the curved line at the lower right of the figure (from Pedersen et al. 1998; see also Figure 3 of Fruchter et al. 2000b).

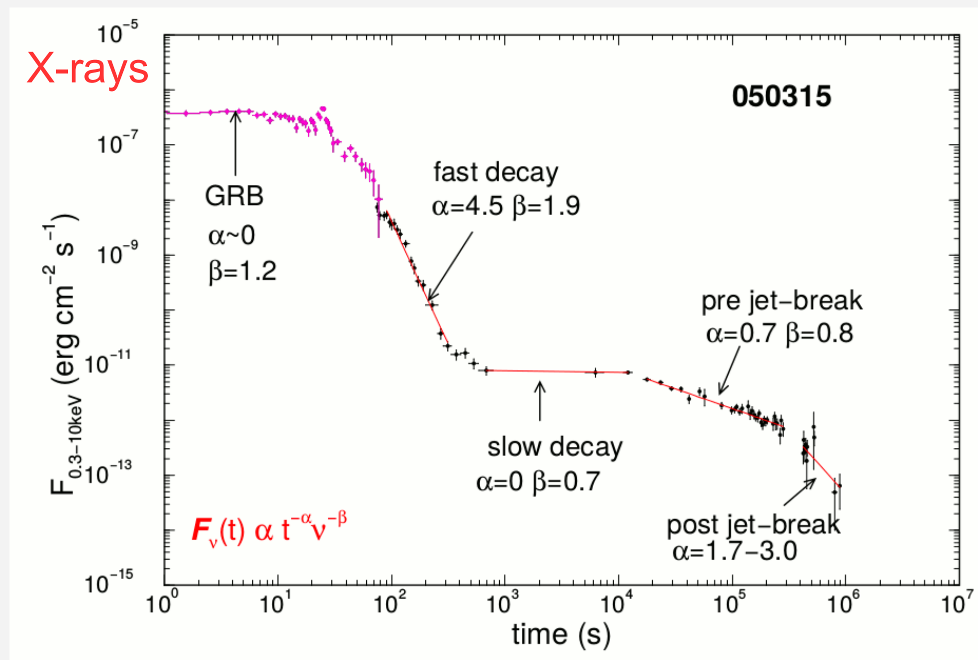

GRBs In a Nutshell

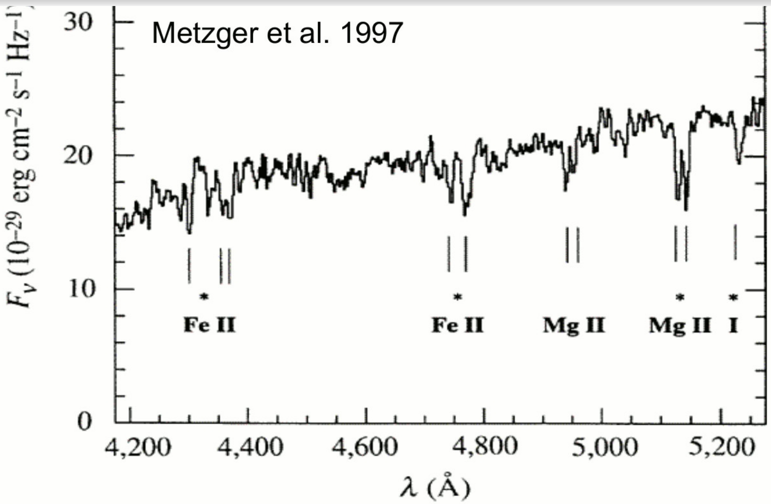

Spectrum of the optical afterglow of GRB970508 with absorption lines at z=0.835.

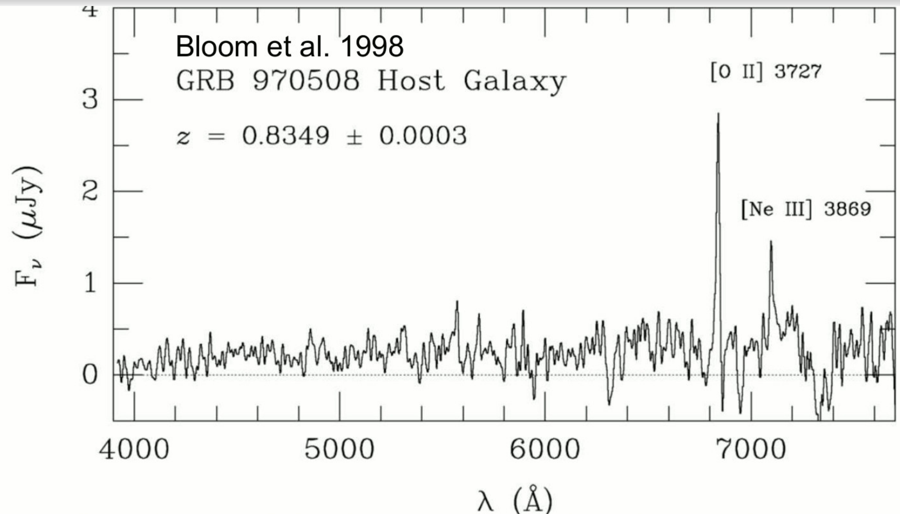

Spectrum of the host galaxy showing emission lines at the same z.

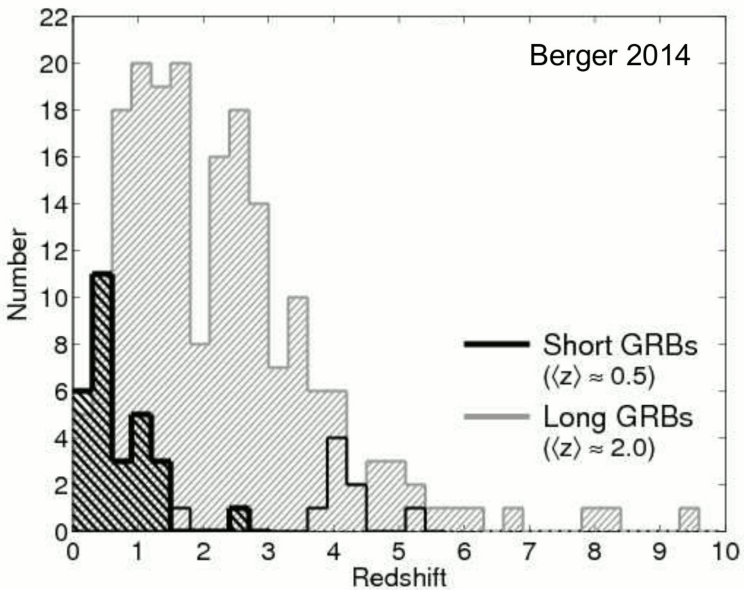

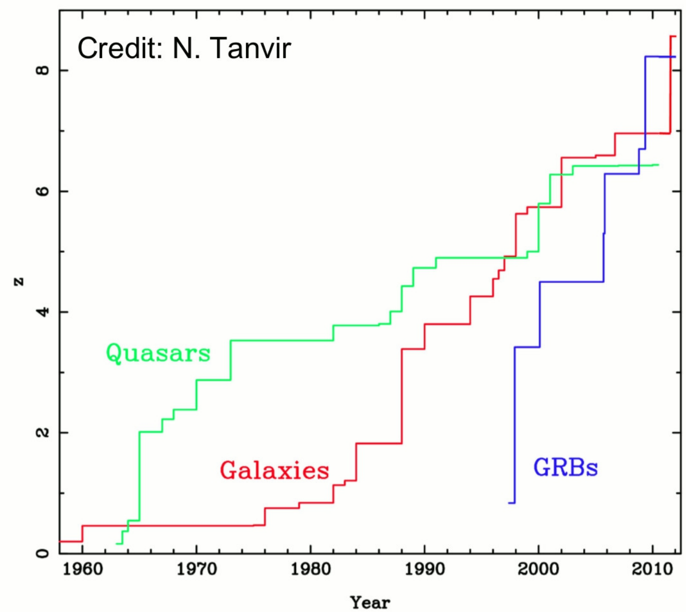

History of discoveries

Least distant observed GRB: z = 0.0085 (GRB980425)
Most distant observed GRB: z = 9.4 (GRB090429B)

GRBs In a Nutshell

Paczynckì & Rhoads 1993; Mezsaros & Rees 1997

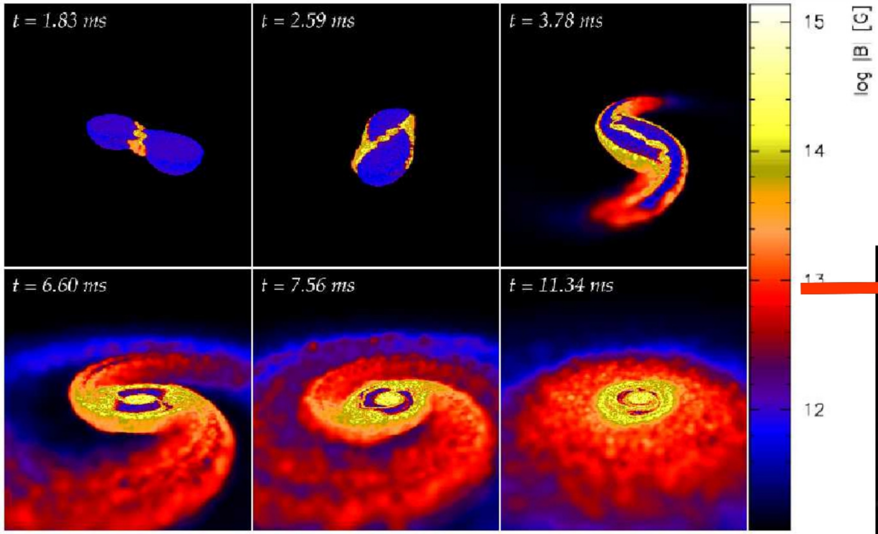

Price & Rosswog 2006

Merger scenario:

Coalescence of two neutron stars

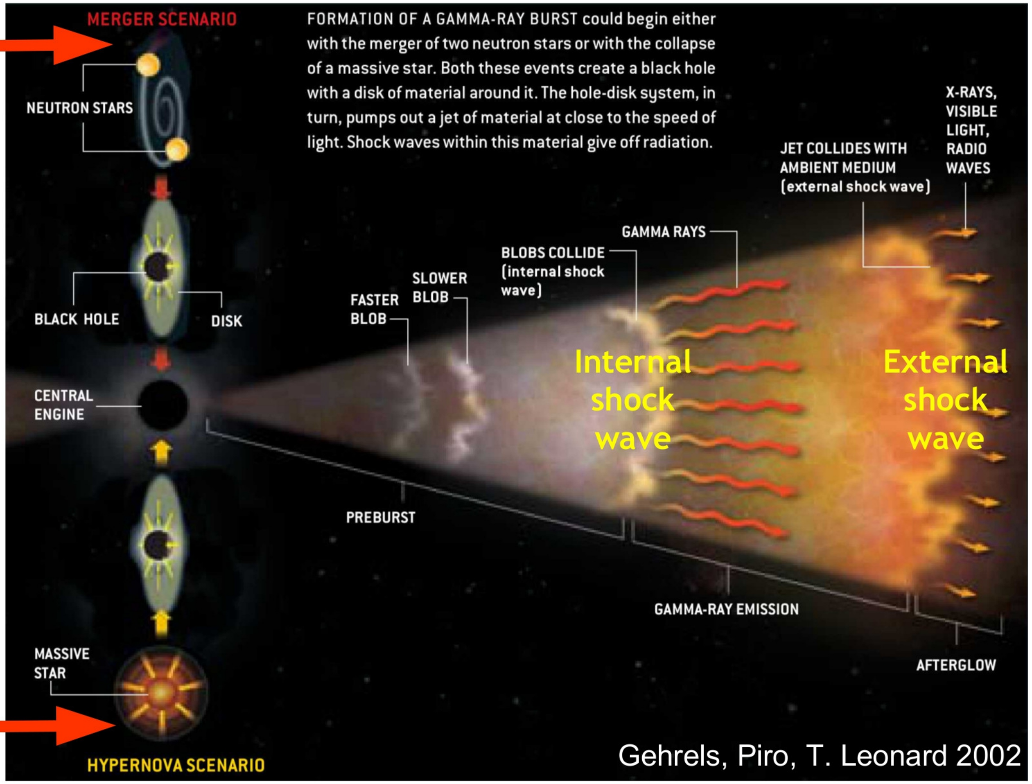

Gehrels, Piro, T. Leonard 2002

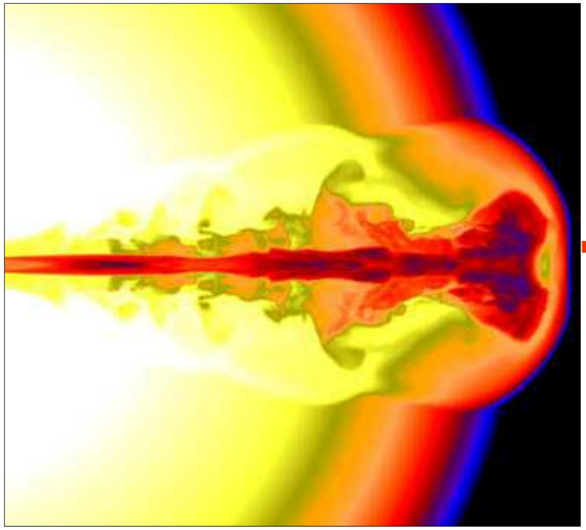

Credit: Zhang & Woosley

Hypernova scenario:

Collapse of a massive star

GRBs In a Nutshell

- The first GRB/SN association was GRB 980425 / SN 1998bw, nearby and very bright type Ic supernova (core-collapse, no He lines). The explosion was unusually energetic, more than 10 times that of an ordinary supernova. GRB 980425 is the closest burst recorded to date with redshift z = 0.0085, i.e. only 37 Mpc.
- Some (not all) long-duration busts are associated with core-collapse supernovae Ic.

GRB 980425 / SN 1998bw

Another example: GRB 041006

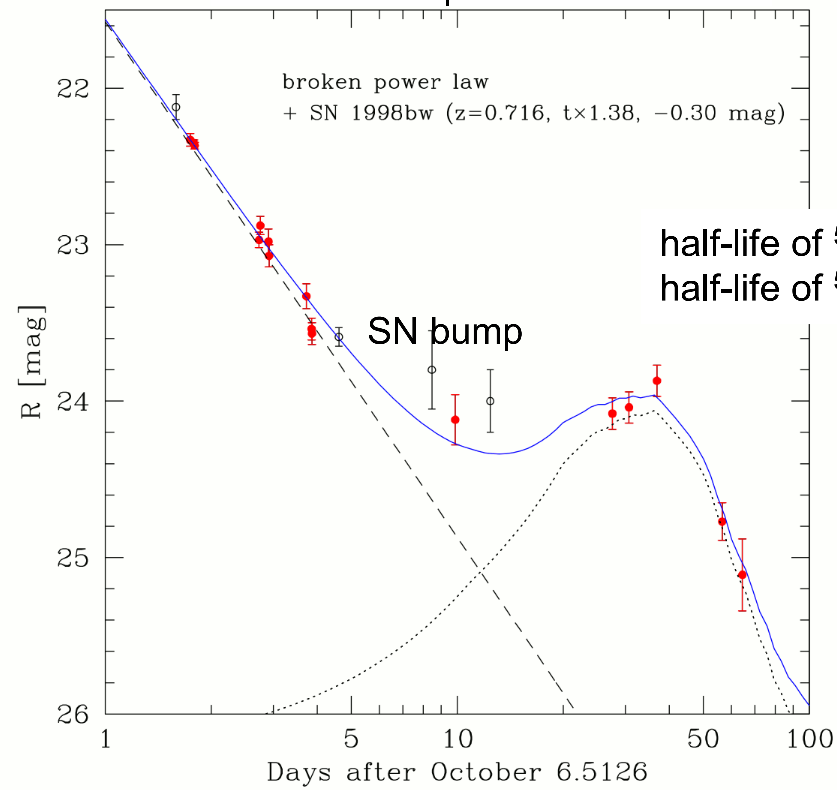

half-life of ^{56}Ni: 6 days
half-life of ^{56}Co: 77 days

The R band light curve of the afterglow of GRB 041006 (red and opened circles denote data from different authors). The power-law decay with a slope of -1.3 is shown by the dashed line. A supernova SN 1998bw light curve extended by a factor 1.38 is indicated by the dotted curve. The solid cure denotes the combination of both components. The supernova bump, powered by the radioactive decay ^{56}Ni $\rightarrow ^{56}$Co $\rightarrow ^{56}$Fe (by K-capture), is clearly evident (Credit: Stanek et al. 2005).

GRBs In a Nutshell

- EM counterpart from NS-NS merger event GW170817/GRB170817A (short duration GRB).
- Large campaign of follow-up observations identified a kilonova.
- Confirmation of short GRBs originating from merger of two compact objects.

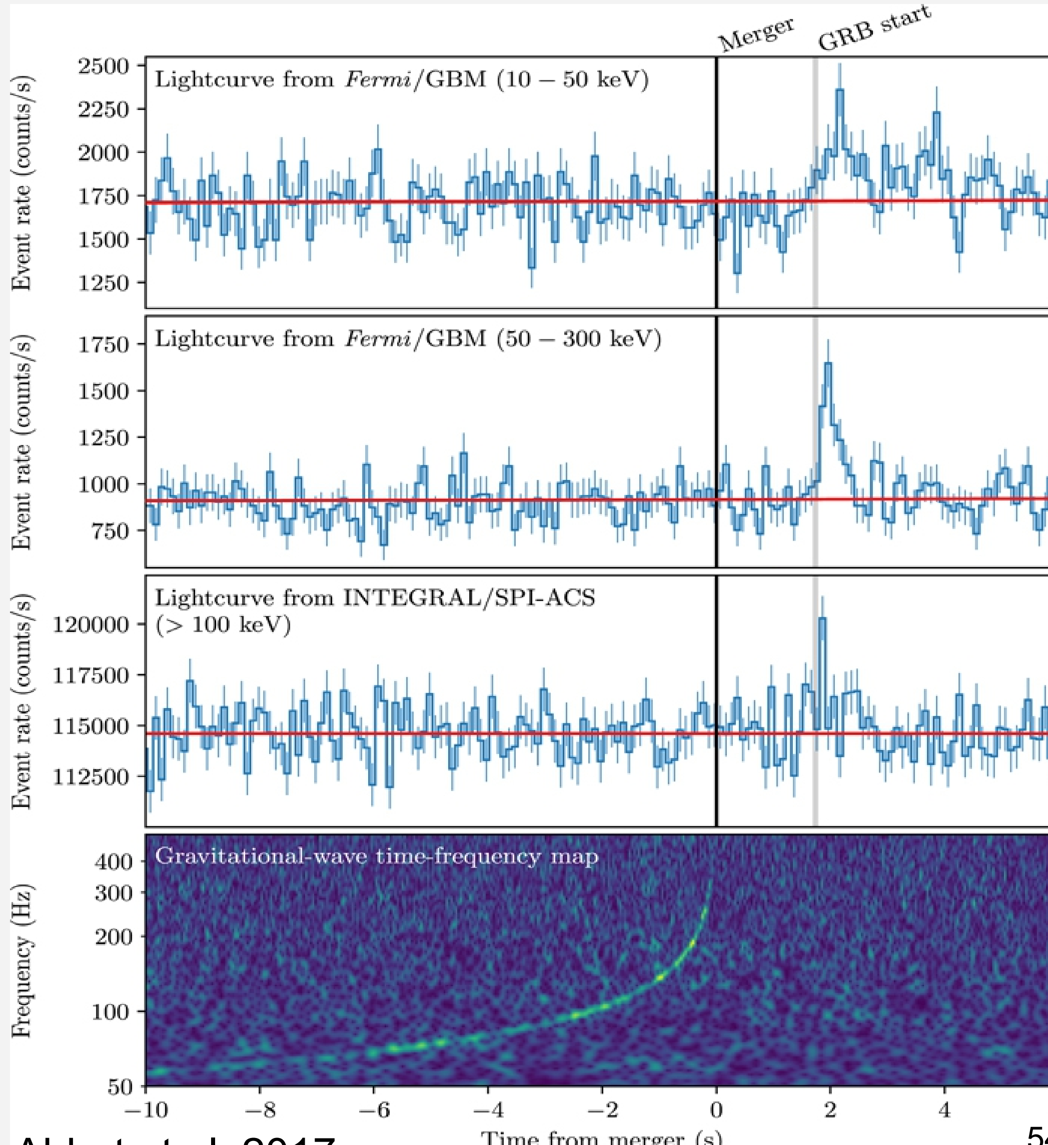

Abbot et al. 2017

Literature

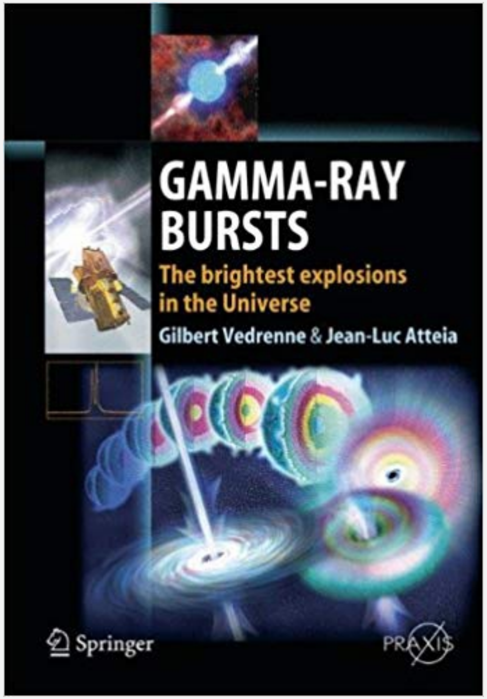

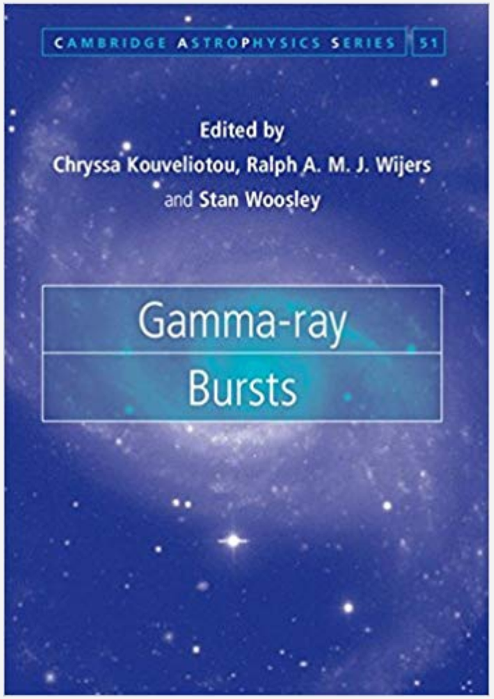

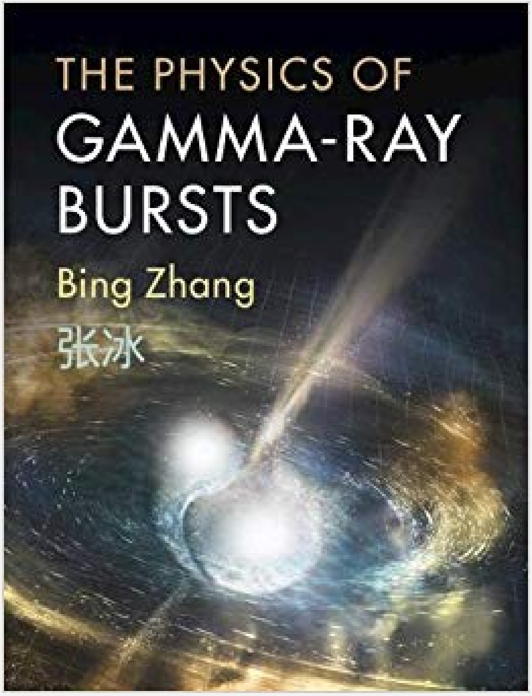

- S. Nagataki 2018, Reports on Progress in Physics, 81, 026901
- Z. Dai et al. 2017, Space Science Review, 212, 409
- P. Schady 2017, Royal Society Open Science, 4, 170304
- P. Willingale adn P. Mészáros 2017, Space Science Review, 207, 63
- F. Piron 2016, Comptes Rendus Physique, 17, 617
- P. Kumar and B. Zhang 2015, Physics Reports, 561, 1
- E. Berger 2014, Annu. Rev. Astron. Astrophys, 52, 43
- N. Gehrels and S. Razzaque 2013, Frontiers of Physics, 8, 661
- A. Gomboc 2012, Contemporary Physics, 53, 339
- P. Mészáros 2006, Rep. Prog. Phys. 69, 2259
- T. Piran 2004, Rev. Mod. Phys., 76, 1143
- P. Mészáros 2002, Annu. Rev. Astron. Astrophys. 40, 137

The End